A stepped frequency continuous wave short range radar for agriculture measurements with coherent cancellation calibration

by

Garrett Sidney Peterson

B.S., Kansas State University, 2015

A THESIS

submitted in partial fulfillment of the requirements for the degree

MASTER OF SCIENCE

Mike Wiegers Department of Electrical and Computer Engineering
Carl R. Ice College of Engineering

KANSAS STATE UNIVERSITY
Manhattan, Kansas

2020

Approved by:

Major Professor
William B. Kuhn

Copyright

Notice: This manuscript has been authored using funds under the Honeywell Federal Manufacturing & Technologies under Contract No. DE-NA-0002839 with the U.S. Department of Energy. The United States Government retains and the publisher, by accepting the article for publication, acknowledges that the United States Government retains a nonexclusive, paid-up, irrevocable, world-wide license to publish or reproduce the published form of this manuscript, or allow others to do so, for United States Government purposes.

Abstract

Leakage/crosstalk in short-range compact radar systems is an issue that is gaining importance as these systems proliferate our society. Leakage and crosstalk in these radars result from three primary sources: antenna, board level, and component level coupling. This leakage/crosstalk often manifests as false targets at the output. Several strategies have been proposed to reduce the effects of these coupling paths. They involve RF cancellation at the frontend of the system, digital cancellation in the backend, or clever antenna placement. All these solutions have limited effectiveness but can be acceptable in given use cases.

This thesis looks at the sources of the leakage/crosstalk and the magnitude each source contributes. It discusses previous research into line isolation to show what can lead to good design decisions and proposes a new method of mitigation that involves injection of a correction signal using the coherent cancellation calibration technique. This technique focuses on short-range stepped frequency continuous wave radar systems. The technique was evaluated through the development and testing of a compact short-range system for agricultural purposes.

The K-State agricultural radar shown went through several revisions and resulted in a compact light-weight sensing radar that shows promise as a sensor for precision agriculture uses. This thesis documents design decisions made in development to produce a radar that can effectively cancel large amounts of self-interference resulting from antenna coupling and mixer leakage. The field experiments show results for measuring crop height and have potential to provide additional data such as yield and biomass estimates.

Table of Contents

List of Figures

Acknowledgements

The author would like to thank Dr. Dallas E. Peterson for his support of this research through the use research plots at the K-State Ashland Bottoms research farm. The author would like to acknowledge the committee members Dr. Don Gruenbacher and Dr. William Hageman for their time and feedback. The author would lastly like to thank Dr. William B. Kuhn for his constant support, encouragement, and continuous guidance throughout his education and research. His outstanding teaching and mentorship has inspired a lifelong passion for learning and engineering.

Dedication

Dedicated to my wife Kelsey.

Chapter 1 - Introduction

1.1 - Current Short-range Radar Systems

Small continuous wave (CW) radio detection and ranging (radar) systems are proliferating in our society. In addition to use as altimeters in aircraft they are used extensively in the automotive industry for advanced safety and convenience features such as adaptive cruise control and collision avoidance [1]. They are also used in industrial applications such as level sensing in fluid tanks, construction projects to find buried wiring and pipes, and even for asphalt inspection [2]. An example of a modern automotive radar system from Bosch can be seen in Figure 1-1(a). Even low cost commercially available stud finders [3] have come onto the market using radar technology, as shown in Figure 1-1(b).

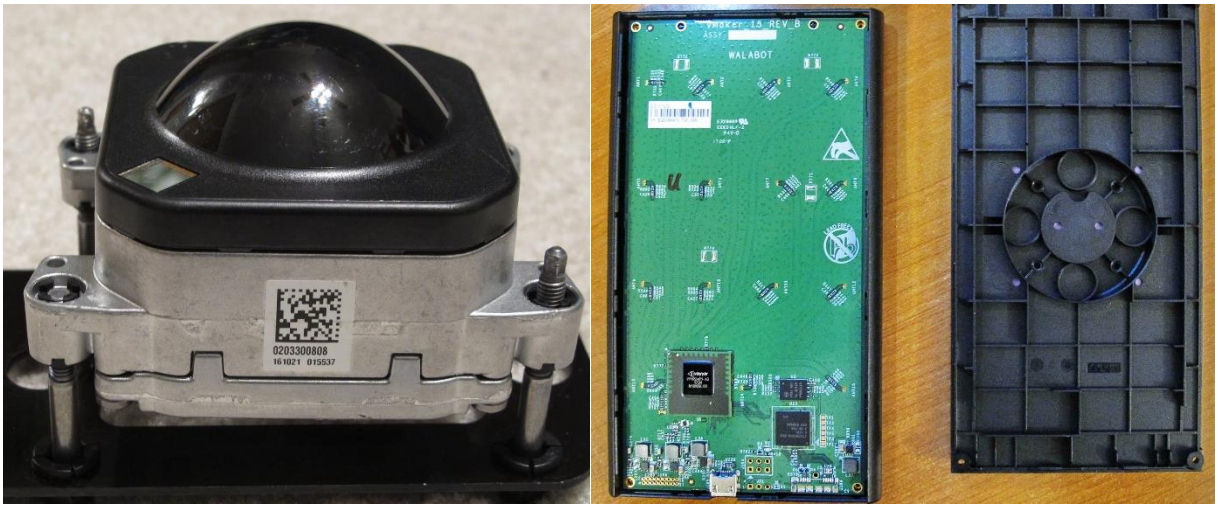

Figure 1-1 -Automotive Radar(a), Stud Finding Radar(b)

The advancement of integrated circuit (IC) processes has led to miniaturization and the low power nature of these devices. By decreasing the lithography size in ICs, higher frequency systems have become possible. Originally implemented in the 4.3GHz band for altimeter applications, newer applications are often in higher-frequency bands. Automotive applications were first focused in the 24GHz UWB (22-29GHz) allocation, but are now shifting to the 77-

81GHz industrial, science and medical (ISM) band. This is a result of different countries regulations of spectrum and the need to homogenize for global marketing [4].

1.2 - Agricultural Need

The world population is projected to exceed 9 billion people by 2050. This increase in population means food production will need to increase to feed an additional 2.3 billion people [5]. Current agricultural production cannot sustain such a large future population. Small short-range radar (SRR) systems can help provide more information about crops and environments to help meet these growing agricultural production demands, providing a useful sensing method for precision agriculture.

Precision agriculture is a growing field that focuses on automation and efficiency in the agriculture industry [6]. Data is the driver behind increasing the efficiency. Knowing more about crops and their environment allows growers to tailor applications of herbicides, fertilizers, and irrigation to use resources more effectively. It also allows growers to better plan future plantings and manage crops in future seasons by establishing a pedigree for fields and crops.

Data commonly collected for precision agriculture use includes soil information (pH levels, moisture content, nutrient levels) and above ground measurements (pest infestations, crop stress levels, weed densities, crop heights, biomass, leaf area index). With a sufficient complement of sensors, data can be collected on a massive scale with thousands of measurements across entire fields. This can allow the grower to pinpoint treatments instead of applying blanket coverage over a field.

The automation push has come from not only treatments but also enhanced data collection vehicle developments. Robotics and drone companies have been flocking to the

agricultural industry [7] and a variety of new systems have been developed to collect more data from fields. Many of these systems have been based on unmanned aerial vehicles (UAV).

Most popular sensing systems have been optically focused using cameras and image processing. The primary issue of this approach has been that since most are taken with UAVs only the canopy can be seen. When taking pictures of the crops from above often the canopy will completely cover the ground. Using a radar system eliminates this obstruction by penetrating the canopy and investigating beneath. There have been P-band synthetic aperture radar (SAR) systems used to measure vegetation on a large scale. These P-band systems are normally used at long range from a high altitude or satellite based. The lower frequency of these systems have good canopy penetration and can reveal large scale changes well, but their range resolution is insufficient for collecting information on the scale of a single plant or smaller. They have been used to look at forest average biomass for example [8], but not the plant's internal structure. With SRR systems operating at higher frequencies with wider bandwidths it may be possible to look at crops in more detail. Possible measurement results include crop heights, moisture content, and biomass estimates at the plant or row level. While these measurements can be estimated from imagery they may be directly measured in more spatial detail using a microwave radar system. For example, a P-band system at 400MHz has a wavelength on the order of 75cm, and a spatial resolution on that scale or larger, depending on system bandwidth. A microwave radar operating at short range could achieve spatial resolution 100 times smaller, potentially providing centimeter scale data and allowing new measurements to improve crop management and yield.

1.3 - Self-Interference Problem

Many compact SRR systems have problems with self-interference, which are not present in longer range systems. This is a result of antenna crosstalk, printed circuit board (PCB) level coupling, and component isolation. In frequency modulated continuous wave (FMCW) and stepped frequency continuous wave (SFCW) radar systems, this self-interference can result in false close range targets and can obstruct weaker returns from more distant targets [9]. If the self-interference is particularly bad this can obscure smaller close range targets or saturate the receiver entirely.

As the demand for smaller short and medium range radars grows, solutions to the self-interference issue are needed. By miniaturizing the systems, components are required to be closer together and the isolation between transmit and receive paths becomes worse. An example of a miniaturized radar system is the K-State agricultural radar that is at the center of this thesis. This radar is shown in Figure 1-2. These problems and others have been addressed with techniques including hardware assisted calibration and careful attention to coupling mechanisms, and will be discussed in subsequent chapters.

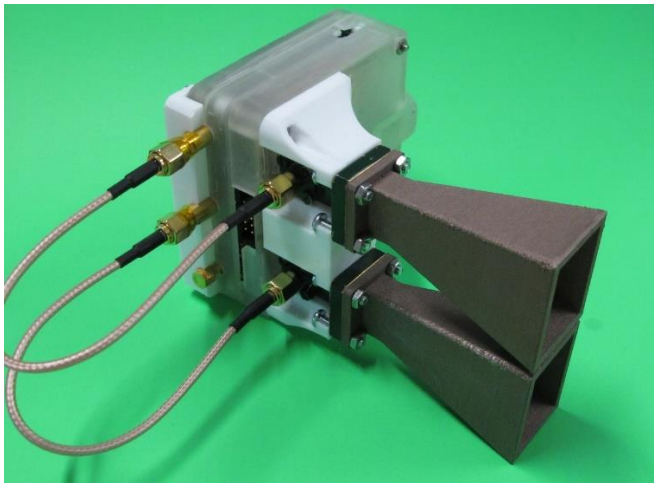

Figure 1-2 K-State Agricultural Radar

1.4 - Prior Work

The most popular approach to correct problems from self-interference is to process the returns at the end of the system in the digital domain [10]. This approach is very similar to moving target indicator (MTI) processing [1]. Since the circuit board and components are ideally static coupling mechanisms, the self-interference should be consistent from sweep to sweep and a simple difference with an empty or previous scene will mitigate the self-interference as long as the receiver is not saturating. However, for a compact SRR system, saturation results when gain is increased to improve sensitivity, and this approach may not be sufficient.

Another technique is to place a phase shifter, attenuator, and coupler from the transmit path to the receive path. The goal is to feed an out-of-phase, attenuated copy of the transmit signal into the receiver and by destructively summing cancel out interference [11]. The main issue with this approach is that is can only account for one leakage path at a specific phase angle. It also requires that the phase shifter and attenuator be variable if the frequency will be swept to account for the phase and amplitude change in the coupling path over frequency.

A third approach deals with antennas that cancel leakage with intentional placement by mounting two transmit antennas in a manner to cancel destructively at the receive antenna. This approach is also bandwidth limited as a result of changing wavelengths over frequency [12].

In contrast, the research documented in this thesis employs “Coherent Cancellation Calibration” (CCC) and related hardware design techniques that can simultaneously mitigate several coupling paths, making a high-sensitivity, high spatial-resolution agricultural radar possible.

1.5 - Thesis Outline

The thesis is divided into six chapters. This first chapter has given a brief overview of current compact radar technologies, limitations of current systems, a review of prior work, and an outline for the reminder of the thesis. Chapter two will provide an overview of typical systems for FMCW and SFCW radar theory and operation. Chapter three investigates the key sources of the coupling mechanisms, including how the mechanisms and specifications impose the limitations in the radar on a system level and details the CCC technique. The fourth chapter will examine the architecture of the K-State agricultural radar system and its' development. Various issues that arose during development will be shown with the outcomes and solutions. Chapter five will give experimental results gathered by the K-State agricultural radar showing the coupling/crosstalk mitigation strategy presented. Finally, chapter six will present the limitations of the coupling/crosstalk strategy implemented and discusses possible improvements.

Chapter 2 - Typical Radar Topologies

Distance measuring radar systems can be divided into two groups, pulsed and continuous operation [13]. Pulsed radars transmit a short-duration pulse and time the duration until an echo is received. This time delay between transmission and reception is used to determine distance. CW radars use a modulation scheme to determine distance. This is normally frequency modulation (FM) for CW radars, or its discrete-time counterpart stepped frequency CW (SFCW). In these systems, the distance is determined from the difference in frequency between the current transmit frequency and the receive frequency, which is a function of the rate of frequency modulation and the radio waves time of flight (TOF) to the target and back. There are also monostatic and bistatic classifications of radar systems where the key difference is if the transmit and receive antennas are shared. The focus of this thesis will be on bistatic SFCW radars and in particular, designs for short ranges. A simplified block diagram of such a radar system is Figure 2-1.

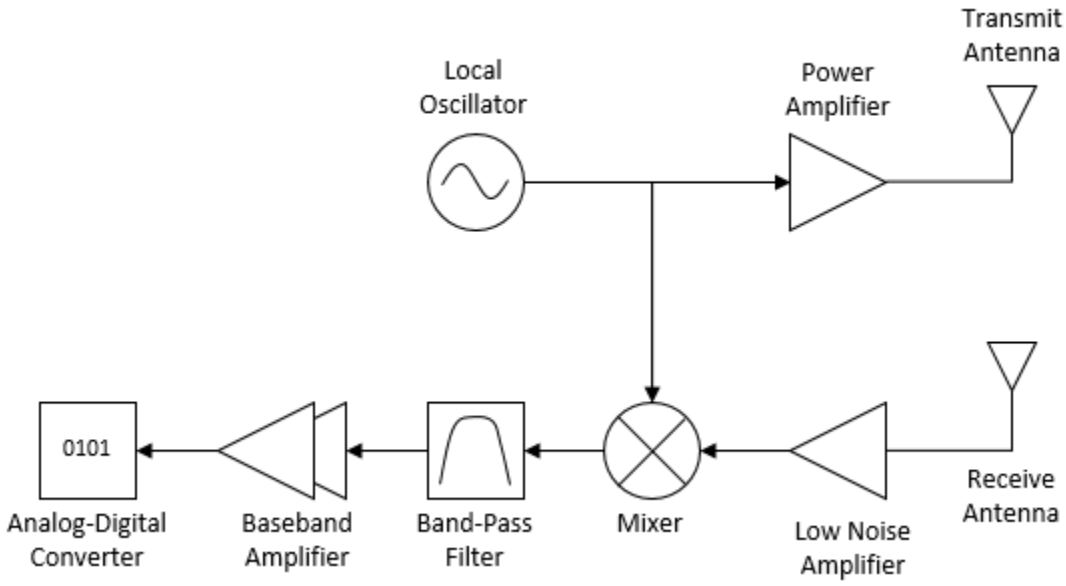

Figure 2-1 Generic FMCW Radar Block Diagram

2.1 - Traditional FMCW Radars

As seen in Figure 2-1, standard FMCW radars use a heterodyne configuration. An FM signal is generated using a voltage controlled oscillator (VCO) whose frequency is swept over a given bandwidth, typically with a voltage ramp. This FM RF signal is then amplified and sent out of an antenna where it travels until it hits a target and is reflected. Various targets/surfaces will reflect varying amounts of energy which can depend on shape, material (conductance or dielectric change), and angle of incidence. Once this signal is reflected it travels back to the receiving antenna where it is amplified using a low noise amplifier (LNA). The signal is then mixed with the transmitting waveform to produce an intermediate frequency (IF) typically in the baseband region (0-1 MHz depending on sweep parameters and target range). During the time it takes the waveform to be transmitted and returned the frequency transmitted has been modulated such that the transmit signal is now at a different frequency than what is received. When the received signal is mixed with the transmit signal this difference in frequency is a resultant IF/baseband sinusoid which contains the range information. This signal is high-pass filtered to reduce self-interference and low-pass filtered to reduce noise and aliasing, further amplified, and digitized.

Normally the transmit signal is modulated in a linear fashion to produce a linear frequency ramp called a chirp. The slope of the frequency ramp is a known value over time and thus the IF/baseband frequency can be used to determine distance with equation (2.1), where f_0 is the IF output frequency, c is the speed of light, and f' is the slope of the frequency modulation.

$$d = \frac{f_0 * c}{2f'} \tag{2.1}$$

The range resolution (ΔR) of this kind of radar system is determined by the bandwidth of the transmit waveform (total sweep width) and can be found using the equation (2.2) with B being the chirp bandwidth [1].

$$\Delta R = \frac{c}{2B} \tag{2.2}$$

This type of radar has a maximum unambiguous range (R_u). Targets outside this unambiguous range may result in erroneous returns due to delayed echoes received in a later sweep. This is constrained temporally by the sweep time found in equation (2.3) with T_s being the sweep time.

$$R_u = \frac{c * T_s}{2} \tag{2.3}$$

2.2 - Stepped Frequency Radars

A related radar topology using a homodyne mixing topology known as SFCW is now gaining popularity. Using a similar process a signal is generated, amplified, and transmitted. The signal travels through the air, reflects off a target, and returns to the receiver. Like in the FMCW radar it is mixed with the transmitted signal, but in an SFCW system the return signal is still at the same frequency. Unlike the FMCW case, the result of this mixing is instead a DC value that encodes the phase difference of the signals. The number of wavelengths between the radar and the target determine this phase difference. A single phase difference by itself is not incredibly helpful because it is only the fractional part of the number of wavelengths, but when the radar is stepped to a new frequency a new phase difference is generated by the new frequency's relationship of range and wavelength. After many phase differences have been collected the result will be a sinusoid whose frequency will relate to the distance. This is similar to the FMCW output, but the IF is now a discrete-time waveform. This can be seen in Figure 2-2 where received amplitude for various frequencies are plotted over distance on the left and the sampled

phases are plotted over time on the right. The vertical arrows represent the IF quasi-DC sampled output values and the dashed purple line illustrates the time smoothed sinusoid that results after lowpass filtering the IF output. This is the same sinusoidal output frequency as in the FMCW case, assuming the same target range and sweep parameters and that enough steps are taken so that no aliasing outside the unambiguous range has occurred.

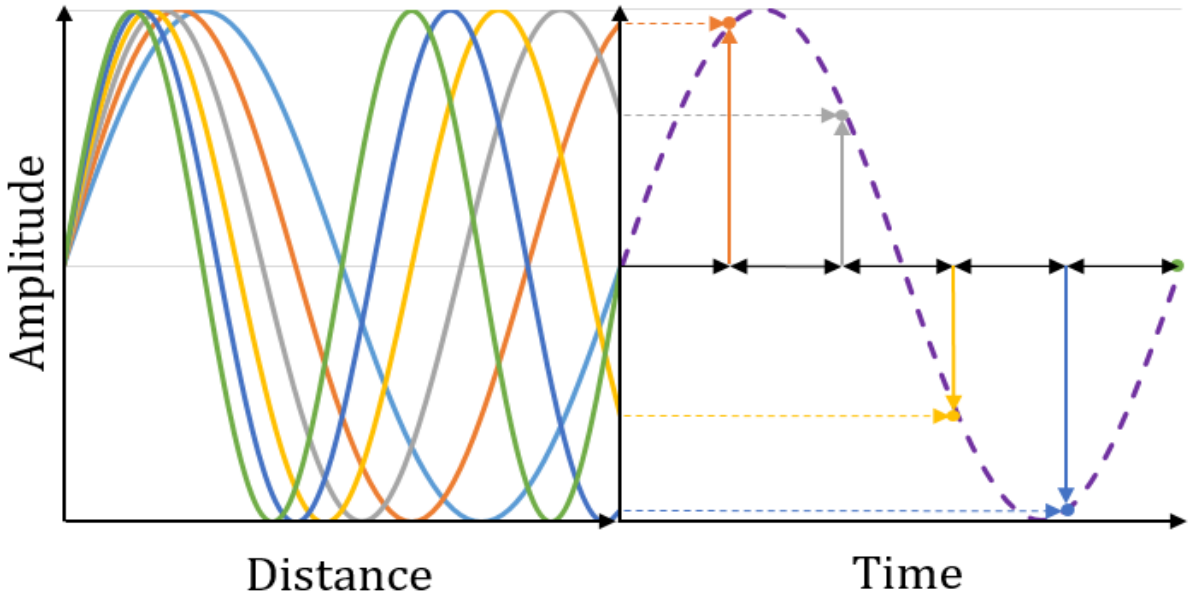

Figure 2-2 SFCW Signal Example

The signal transmitted from the radar at a given step n can be described as $s_T(t)$ with a frequency f_n:

$$s_T(t) = A_T \cos(2\pi f_n t) \tag{2.4}$$

with A_T the amplitude and the time step is assumed to begin, without a loss of generality at $t = 0$.

This signal is received by the radar beginning at $t = t_p$ where t_p is a range dependent propagation delay determined by distance d to the target. The received signal $s_R(t)$ may be described (for $t > t_p$) by:

$$s_R(t) = A_R \cos\left(2\pi f_n\left(t - t_p\right)\right) \tag{2.5}$$

where $A_R$is the received amplitude determined by the path loss and the targets radar cross section (RCS). At step n, these two sinusoids differ in phase by an amount:

$$\phi_n = -2\pi f_n t_p \tag{2.6}$$

Following the mixing in the receiver and lowpass filtering, this will produce a DC output for the duration of frequency step f_n as:

$$v(n) = \frac{1}{2} A_T A_R \mathrm{K}\cos(-2\pi f_n t_p) \tag{2.7}$$

or,

$$v(n) = A_{IF}\cos(\phi_n) \tag{2.8}$$

where K models gain within the receiver and A_{IF} represents the quasi DC amplitude after gains have been applied to the signal.

The phase (ϕ_n) is related to the propagation time t_p and the current frequency f_n according to (2.6) wherein the propagation time can be determined using the velocity of propagation (speed of light for a vacuum) c and the distance (d) as:

$$t_p = \frac{2d}{c} \tag{2.9}$$

For cases with $f_n t_p > 1$, ϕ_n is greater than 2π, and t_p cannot be found uniquely from a single value of $v(n)$. However if the frequencies of f_n are sufficiently closely spaced, then the phase delta between steps given by:

$$\Delta\phi_n = 2\pi f_{n+1} t_p - 2\pi f_n t_p \tag{2.10}$$

$$\Delta\phi_n = 2\pi(f_{n+1} - f_n)\, t_p$$

$$\Delta\phi_n = 2\pi(\Delta \mathrm{f}) t_p$$

will be less than 2π, and t_p can be uniquely found. To avoid aliasing $2\pi(\Delta \mathrm{f})t_p < \pi$ must be true which leads to:

$$t_p < \frac{1}{2(\Delta \mathrm{f})} \tag{2.11}$$

Combining with (2.9) gives us an expression for unambiguous range in a SFCW radar:

$$\frac{2\mathrm{d}}{\mathrm{c}} < \frac{1}{2(\Delta \mathrm{f})} \tag{2.12}$$

$$\mathrm{d} < \frac{\mathrm{c}}{4(\Delta \mathrm{f})}$$

$$R_u = \frac{c}{4(\Delta \mathrm{f})}$$

Equation (2.8) can be recognized as a discrete-time sinusoid:

$$v(n) = A_{IF} \cos\big((\Delta\phi)(n)\big) \tag{2.13}$$

produced from the sequence of frequency steps during the radars frequency sweep, where $\Delta\phi$ is the difference in phase between consecutive sample points in the sweep. Given sufficient constraints on target range, frequency step size, and sample rate, the frequency of this discrete-time sinusoid can be directly related to the baseband sinusoid output frequency in (2.1) produced by a traditional FMCW analog sweep.

The bandwidth of an SFCW radar can be related to the frequency step size $\Delta \mathrm{f}$ and the number of frequency steps N as:

$$B = N\,\Delta \mathrm{f} \tag{2.14}$$

This can be used to relate back to the range resolution ΔR as in equation (2.2).

2.4 – SFCW Design Example

This subsection illustrates operating parameter requirements for an SFCW systems based on the equations derived in the previous section. We will target the following system

requirements an R_u of 10 m and a ΔR of 10 cm. Using equations (2.2), (2.12), and (2.14) allows us to solve for the minimum bandwidth and frequency step size as:

$$B = \frac{3 * 10^8}{2 * 0.1} = 1.5GHz \quad \text{from (2.2)}$$

$$\Delta \text{f} = \frac{3 * 10^8}{4(10)} = 7.5MHz \quad \text{from (2.12)}$$

$$N = \frac{1.5 * 10^9}{7.5 * 10^6} = 667\ steps \quad \text{from (2.14)}$$

These lead to the analog RF section system requirements, but there are still some additional important requirements regarding the digital sections. It is important that the target remain at a static range during the measurements and so all the measurements must be taken in a reasonably short time period. To ensure things are relatively static in an agricultural setting where wind acts on plants, we will assume a measurement time period of 1/1000 of a second. This means the system needs to take 667 steps in a 1mS time frame, resulting in a sample period of 1.5 microseconds, leading to a sample rate of 667 ks/s. These sampling requirements impact hardware system decisions such as ADC sampling rate, frequency settling time, and filtering corners, and were used in the agricultural radar development documented in Chapter 4.

2.5 - Multi Target Scenarios

In the previous subsections, basic functionality of FMCW and SFCW radars were described. Effectively both types of radars have the same output, a sinusoid whose frequency contains range information. Issues arise when the theory is put into practice in the real world, however. In particular, multipath and returns from multiple targets pollute the spectrum. Instead of receiving one pure tone at the radar's output, the result will be a full spectrum in any real world environment. This can make finding a target of interest difficult. Another issue is the information used to determine the frequencies of the output is finite. This falls back to the range resolution equation (2.2) that only a finite bandwidth is available. From Nyquist theory it

requires an infinite number of frequency components to perfectly recreate a signal with a finite time duration that results from any sampling window applied.

In Figure 2-3 a different number of points are used to calculate each spectrum. There are two targets, one at 2kHz and another at 5kHz. The 2kHz target is 20dB larger in amplitude. At the lower sample count in blue, the smaller 5kHz target is largely obscured by the larger lower frequency target. As the sample count is increased the smaller target is uncovered from the large low frequency return.

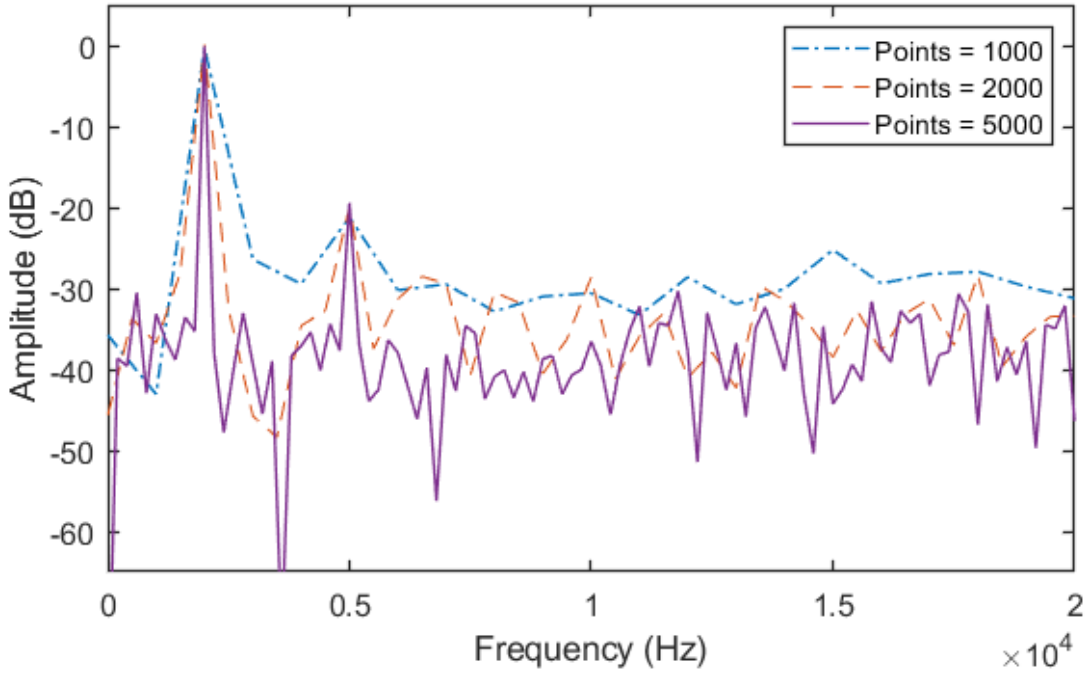

Figure 2-3 Windowing Target Covering Example

This is a problem for the radar systems described because the sample points are limited by the bandwidth of the radar. Another issue occurs from the angles of returns that cause a single physically large target to generate returns over a swath of distances.

These issues are compounded by the leakage paths in the system which will generally look like large close target returns and can be so large they cover the targets of interest. This is

the motivation for the coupling mechanism research and ultimately the mitigation strategies that suppress the self-interference caused by coupling, which are the subject of the next chapter.

Chapter 3 - Coupling Mechanisms and Components

This chapter overviews coupling mechanisms in compact radar systems and component specifications that are related. Coupling leads to leakages/crosstalk between the transmit and receive paths of the radar, which limits performance such as the radars dynamic range and sensitivity as illustrated in the previous chapter. The level of coupling can be measured using a network analyzer looking at S21 or S12, which are measures of the gain/attenuation between two different ports. By examining the isolation of different mechanisms in the system, key paths were determined and addressed in the radar development. A block diagram showing the leakages described in the system can be found Figure 3-1.

Mechanisms in this chapter are broken down into three areas: antennas, board level (e.g. line leakage), and component level (e.g. mixers). Lastly we will look at how these coupling mechanisms are normally dealt with in different radar systems and introduce the CCC technique developed for the K-State agricultural radar.

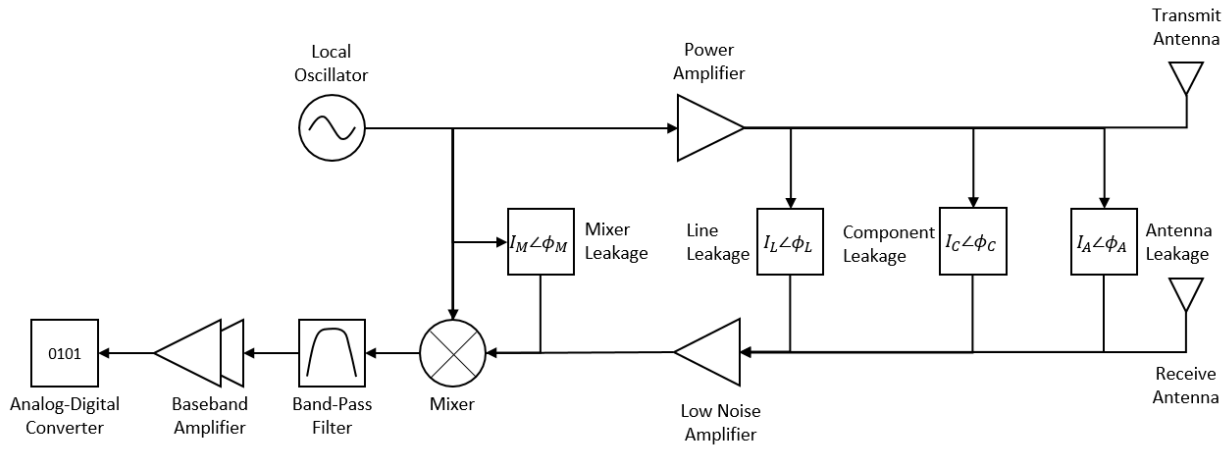

Figure 3-1 Simple Radar Block Diagram with Leakage Paths

3.1 - Antennas

Antennas are normally specified in terms of input impedance, return-loss, gains, and patterns. Input impedance and return-loss for an antenna used in transmit mode come from the ability to convert whatever the feed's characteristic impedance is into the characteristic impedance of free space. This generally will not work over all frequencies and as a result, the antenna will have a specific band of usable frequencies. Most designers look for a 10dB return-loss in the desired band of operation meaning 90% of the power is radiated. How effectively that power is sent from the antenna to a specific direction is a measure of the directivity gain. This is most commonly measured in dBi which compares an antenna's directionally to an isotropic radiator. A good way to imagine this gain is to think of an isotropic radiator as a perfect spherical balloon and an antenna will squeeze that balloon so that it will extend in a specific direction at the expense of others. Some common hypothetical antenna gains are 2 dBi for a dipole, 3dBi for a patch, 5 dBi for a monopole above a ground plane, and typically greater than 10dBi for horn antennas. Since these gains are measured over angles an antenna pattern is associated with the gain.

Antenna crosstalk/leakage occurs in an FMCW or SFCW radar system when two antennas are employed, one for transmit and one for receive. Antenna crosstalk/leakage is the result of placement, nearfield coupling, and/or pattern, depending on the separation distance relative to the antenna size. When antennas are spaced very close together, near field coupling can occur. This usually dominates pattern effects on coupling when the separation between antennas is less than two wavelengths for antennas that are not electrically large. This occurs because the traveling waves have not yet constructed a unified wave front. When two such antennas are separated by greater than two wavelengths (or in general by the Fraunhofer

distance) a signal transmitted by one will be received on the other as the electromagnetic wave propagates through space based on the far field antenna pattern. In the compact SRR developed in the current research, near-field coupling dominates and simulations and/or measurements are required to determine the coupling value.

As a specific example, the horn antennas used on the K-State agricultural radar shown previously in Figure 1-2 exhibited a nominal isolation of 70dB in the band of interest. A test setup using a network analyzer and the measurement results can be seen in Figure 3-2. The result was generated by first normalizing the loss, placing the antennas touching and directly facing each other and calibrating so measured result was 0dB. Some smaller antennas such as lower-gain horns and path arrays showed isolation values in the 40-50dB range in similar tests. In either case the coupling is significant enough to limit the radar's sensitivity, and must be addressed.

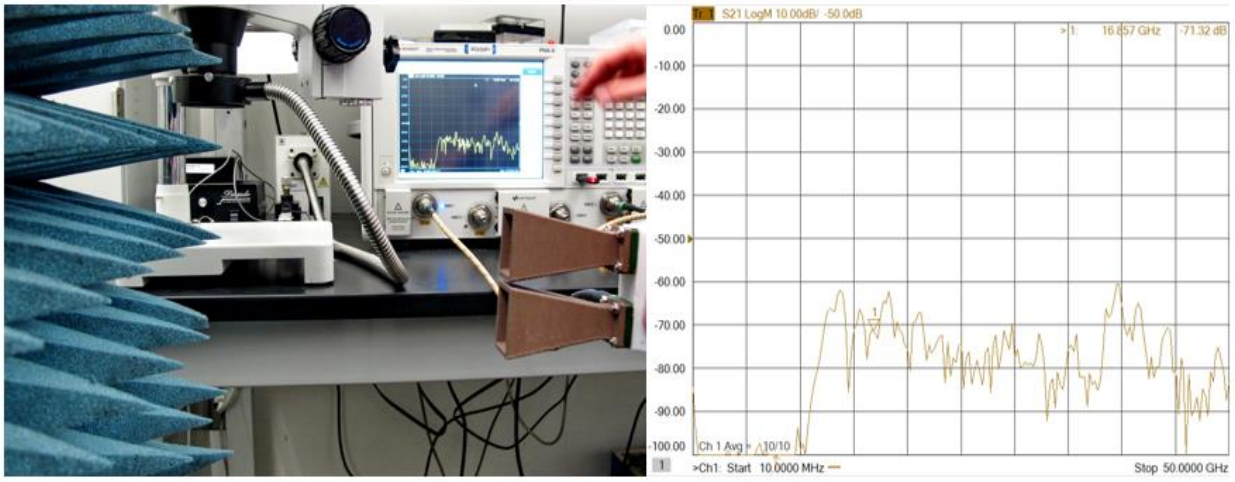

Figure 3-2 Antenna Isolation Measurement Setup and Results

3.2 -Board Level

Modern electronics are created on PCBs which are created with layers of conductors spaced with dielectrics. These dielectrics are often referred to as the substrates. Substrates are defined by the materials they are composed of but in general are characterized by a dielectric constant and loss tangent. This constant describes the relative permittivity compared to a vacuum, controlling the speed an electromagnetic wave can propagate through the material. This can help determine wavelengths of electromagnetic (EM) waves in the substrate. The loss tangent gives designers a measure of how much the traveling wave will be absorbed by the material as it propagates. Both of these specifications, together with signal trace separation affect the isolation achievable in a given substrate.

On a PCB, traces at high frequencies can also couple by becoming radiators. It is known when the wavelength of a signal travelling along a trace becomes similar to the length, designers should treat it as a transmission line. Some previous studies [14, 15, 16] have shown couplings between traces ranging between -30dB to -100dB depending of the type of line used, the length, and the spacing. The most common type of transmission line is microstrip, which is a trace above a ground. Microstrip has been shown to provide the worst performance in terms of isolation of common transmission line topologies, since propagating fields are not well contained above the substrate and trace. Another common type is coplanar waveguide with ground (CPWG) which is created using a topside ground flood flanking the signal trace and walls of vias connected to a ground plane underneath the signal trace. CPWG generally provides better isolation than microstrip because fields are better contained both above and below the trace. A third type, stripline has been shown to provide the best isolation. This is classically created by placing the signal trace on an internal layer in a PCB and positioning ground planes above and below. For

best performance, stripline can be flanked by grounded vias to create a pseudo coaxial structure – sometimes called “rect-ax”. Ideally, this can be a nearly fully-enclosed structure with very high isolation, but isolation is limited at the signal launch and load where the enclosure is broken [17]. Some example diagrams of the three line types can be found in Figure 3-3.

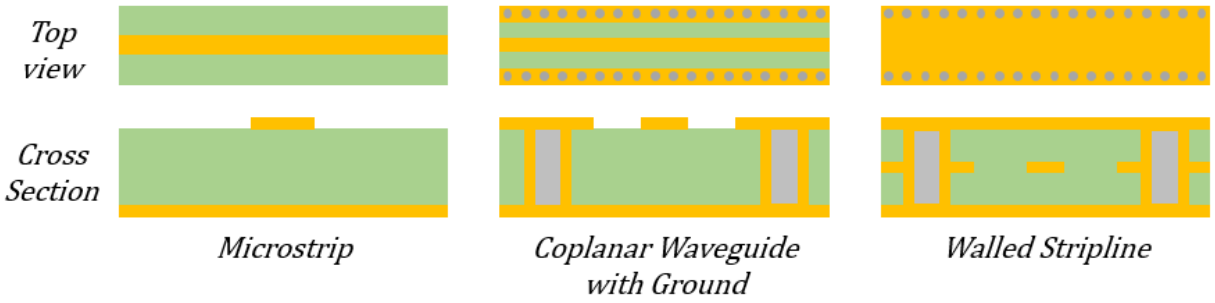

Figure 3-3 Common PCB Transmission Line Types

It was shown that between two microstrip transmission lines separated by 150 mils far end crosstalk/coupling (FEXT) resulted in 30dB of isolation at frequencies above 10GHz compared to 45dB for CPWG with similar distances, while stripline can show up to 70dB of isolation if not compromised by field leakages at the launch and endpoints [17]. This line leakage is depicted in Figure 3-1 as an attenuation and phase shift block in connecting the power amplifier output and the LNA input but could occur at multiple places between the many transmission lines in a system. Nominally, the leakage attenuation can be estimated as 40-50 dB for purposes of assessing coupling in a design. This can dominate or be of similar levels to the antenna coupling seen earlier in Figure 3-2 and suggests attention should be paid to this mechanism in a design.

3.3 - Component Level

Another leakage path between transmit and receive chains can occur within components themselves. In homodyne receiver architectures, the received signal is directly down converted

by mixing it with the transmit signal. Mixers are one of the primary sources of component level coupling. This is a result of a direct path between the transmitted signal and the received signal through parasitics and circuit imbalances in the mixing devices.

There are various mixer architectures that provide different amounts of isolation such as single-balanced, double-balanced, sub-harmonic, and image reject to name a few. They are generally broken down into passive versus active topologies, and each type has different performance with respect to isolation. Common commercially available mixers which are generally dominated by the double-balanced topology have isolations between the RF/LO port of between 20-50dB. There are few examples of commercially available isolations greater than 60dB. In Figure 3-1 the mixer leakages are shown as an attenuation and phase shift blocks connecting the mixer local oscillator port and RF port. This can result from an immediate mixing of the leakage or can result from a reflection off the LNA output. This is a commonly overlooked problem. An often overlooked path occurs when signal leaks through the mixer, travels through LNA, reflects off a receiving antenna, and returns to amplify back through the LNA and mix down at a higher level.

Another component that is a common source of coupling are inductors. Often miniaturization has led to fully integrated radars where a majority of the radio frequency (RF) components are integrated onto a single IC. While there are many advantages to that level of integration a major drawback is the coupling it produces. Amplifiers that are in transmit and receive paths often require matching components that include an inductor. Having inductors physically close on an IC can create coupling paths. This can result in the same interference the mixer leakage produces by directly coupling some of the transmitted signal into the receiver [18]. Some internal component leakage is shown in Figure 3-1 at the output of the PA and LNA

input in Figure 3-1 to symbolize components in amplifiers that could be inductively coupled. This coupling path can easily limit a design's overall performance if not carefully assessed during an IC design and addressed. Careful EM-level simulations may be required in an IC design to characterize this coupling.

3.4 - Coping Mechanisms

The coupling mechanisms described all lead to similar effects of having the transmitted signal appear directly at the receiver, often at a strong level relative to over the air returns. This will result in spurious close range targets once the received signal has been processed, which can mask weak returns from actual targets as discussed in section 2-5. Designers must work to minimize coupling in the hardware design as much as possible through careful subsystem modeling, simulations, and realizations. For example, in PCB layout, the paths shown in Figure 3-1 must be considered and good choices of transmission line type and signal launching must be taken into account. In the IC case, counter-wound inductors could be employed in differential LC tanks, or other methods such as employing on-chip transmission lines in resonators could be considered. At the system and packaging level, the type and location of antennas is important. In the end however, it may not be possible to exceed 50 dB or so of isolation and methods of dealing with this limited isolation are critical to radar success. Commonly there have been three primary approaches to deal with the problem.

One approach is to couple some of the transmitted signal into the receiver [11]. While this may at first appear to make things worse, by phase shifting and attenuating the coupled signal it is possible to destructively interfere with the undesired signal. This approach is commonly known as RF cancellation or neutralization [19]. There has been much interest in this approach in terms of self-interference cancellation for full duplex communication. This has also

been investigated for monostatic operation of systems that were normally bistatic [10, 11]. The primary issues with this approach are that effective nulling is typically limited to about 20-40dB improvements and that unless multiple coupling paths are established only one leakage can be cancelled because the leakage only cancels at one specific phase. This can be problematic if there are multiple coupling sources providing significant interference. One advantage of this option is that since the signal can be cancelled before the received signal is amplified it can cancel out very large leakages that may saturate the receiver versus other approaches.

The second approach more commonly applied is to handle leakages in the digital domain. Since the leakage will be constant, the undesired IF/baseband outputs that result from these paths can be characterized and recorded. Once characterized the leakage effects can simply be subtracted away in the digital domain. This approach is very cost effective and easy to implement in most systems. However, the issue with this approach is that since the leakage needs to be characterized in the digital domain the signal must never saturate at any point in the receive chain. If the signal saturates there will be no recovering the true information. This leads to adding a limited amount of gain in the receiver and normally decreases the sensitivity of the system. Whether this loss of sensitivity is acceptable or not depends on the system's application.

There are also some physical mechanisms to deal with capacitive and near field couplings on the board. One is to physically separate the lines and sections for the transmitter and receiver. But as the push for miniaturization progresses it becomes prohibitive to make the system larger. Another improvement can be made by adding absorbing materials. This material is made out of ferrite loaded silicon most commonly [20].It should be placed close and above the offending lines to mitigate radiation from the lines and near-field EM coupling. This approach adds some

cost and some additional mechanical design constraints, but can be used to augment some of the other approaches described.

A last possible mitigation is possible by simply high pass filtering the lower frequency coupling-based spurious returns. It can be as simple as a capacitor in series with the output of the mixer. Unfortunately, while feasible for medium and long range radars this has problems for SRR systems. For SRR systems it is hard to get an appropriate frequency response that eliminates the coupling while not interfering with the target frequencies of interest.

3.5 - Coherent Cancellation Calibration

In this research, a combined hardware and software solution is applied: Coherent Cancellation Calibration [21]. The key component of CCC is the ability to null out virtually all self-interference leakage while allowing high baseband gain for optimum sensitivity. This is accomplished by adding a correction signal into the receiving chain before significant amplification. The CCC signal injection should occur immediately post mixing to counteract the largest signal possible. A simplified block diagram showing a system with the CCC injection point can be seen in Figure 3-4.

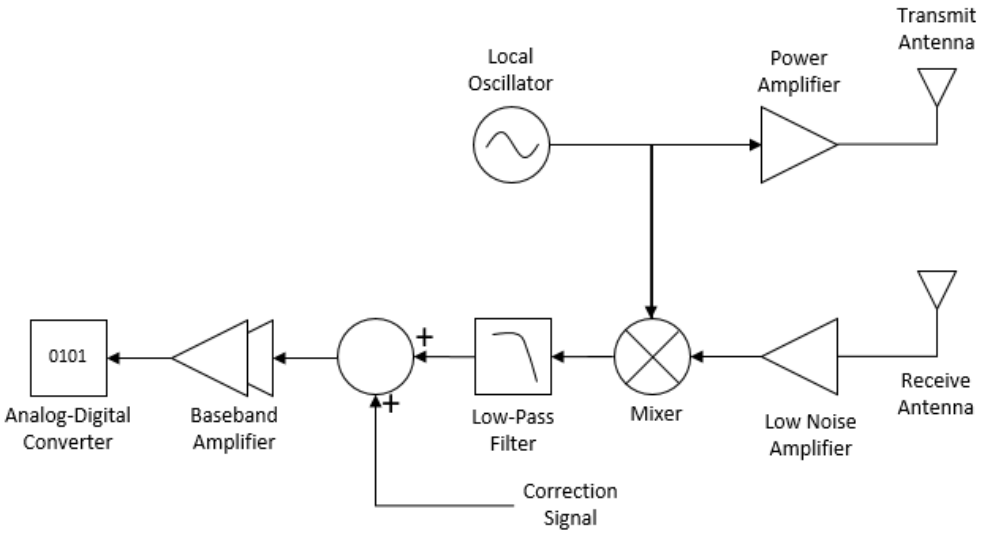

Figure 3-4 Simple Radar Diagram with CCC Injection

The concept behind the CCC corrections is that a blank scene is captured. A blank scene can be captured in an anechoic chamber or by pointing the radar toward an empty sky. The frequency is stepped as it normally would be for a SFCW radar. The return captured will contain low frequency components that are a result of the different leakage paths previously discussed in this chapter. Once the return is captured and stored it can be used to feed an inverse signal back into the receiving chain to destructively interfere with the system self-leakage.

Since the sweep is over the same frequency steps and the components and leakage paths are reasonably static, this can also account for many different leakage paths, as the blank scene is a summation of all the system leakage. This calibration can be applied continuously to sweeps after it has been completed. In our implementation, we have observed that there are some caveats due to drift that can occur in the system over time and recalibration may be required, but the technique has proven to be reasonably robust as illustrated in the experimental results presented in Chapter 5.

Chapter 4 - K-State Agricultural Radar Development

The K-State agricultural radar has been through many revisions to overcome various issues and improve performance. The current revision can be seen on the right in Figure 4-1. It is an SFCW radar that operates in 25 GHz band (nominally 23.5-26.5 GHz) with one transmit and two receive channels. The total system consumes only 1.5 watts during operation. The fully packaged system pictured previously in Figure 1-2 weighs 340g with battery, case, and antennas. The development was started in fall of 2016. The first version of the system was fabricated in February 2017 and can been seen on the left in Figure 4-1. Most of the evolution in the system has came on the digital/control side with the analog and frontend electronics remaining largely the same, with exception of the frequency synthesizer.

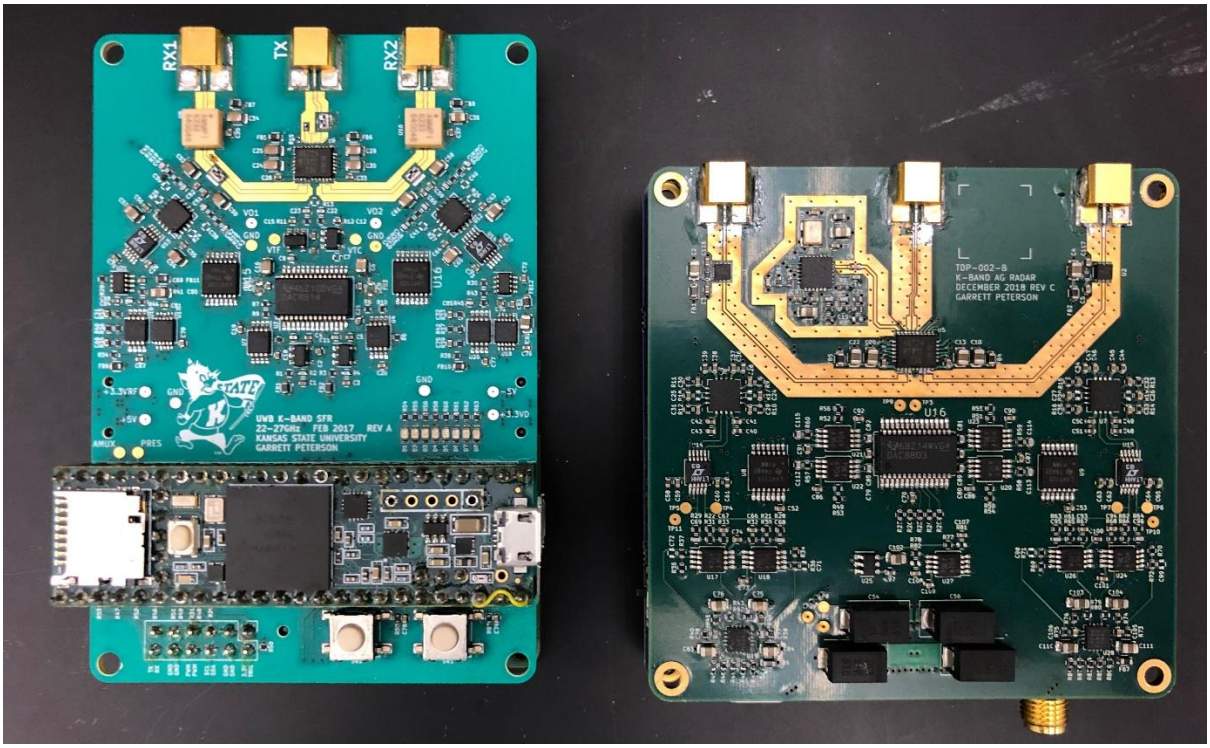

Figure 4-1 K-State Agricultural Radar Circuit Boards

4.1 – K-State Agricultural Radar Overview

The radar was built around the Infineon BGT24MTR12 chipset which includes transmit/receive amplifiers, quadrature mixers, frequency dividers, and a VCO. The core chipset generates the signal and is then amplified to a 0dBm level inside the core chip before it is transmitted. The received signal is then amplified by an external LNA before being down converted in the core chip to produce the IF/baseband output waveform. The CCC is then applied before this baseband signal is amplified and digitized, and sent to the digital section for storage. Once a frequency ramp is complete the sampled phases are sent to a computer for processing. The computer performs the processing to determine target distances using an FFT on the output waveforms.

What made this radar unique from normal radar systems is the addition of a summing amplifier in the receive chain that allowed for Coherent Calibration Cancellation (CCC). This radar system was the initial physical test for CCC [21]. The position of the correction waveform injection was specifically chosen in the receive chain as too maximize the dynamic range while still dealing with large self-interference. It is important that some early gain from an LNA is used to set an acceptable system noise figure, but corrections need be applied as early as possible after to allow the injected correction signal to correct for large signal levels of self-interference. The earlier in the chain the CCC correction is applied the larger the signal can be calibrated out. In this radar the correction is applied immediately following the mixing. A block diagram of revision C of the radar can be seen in Figure 4-2. Note that the baseband processing path is totally DC coupled. This allows the agricultural radar to be used at very close ranges on the order of 10 cm or less if desired.

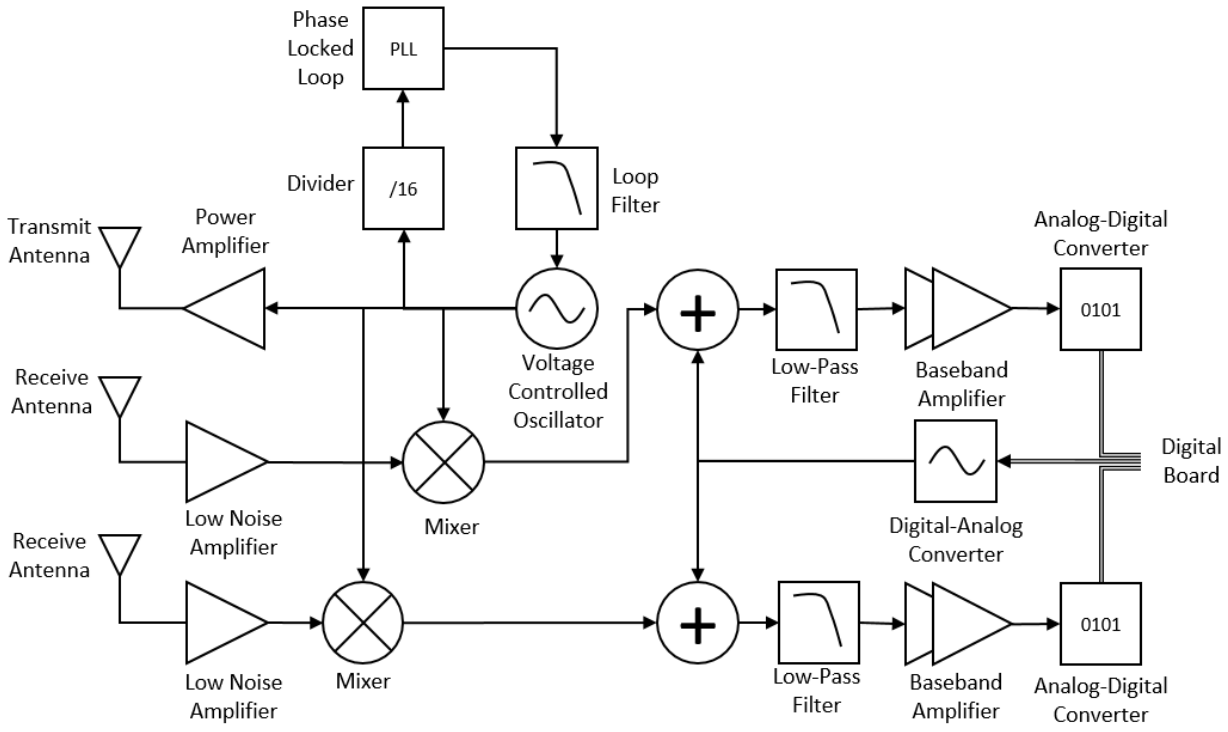

Figure 4-2 Analog Radar Board Block Diagram

In this radar the correction was applied with an offset injected into an instrumentation amplifier. The correction signal is generated by a 14 bit DAC. The resolution of the DAC will inject some quantization noise into the system so a higher resolution DAC performs better. There is a trade between the resolution and speed of the DAC. The speed requirement is set by the sample rate of the ADC and ultimately the sweep time of the radar.

At the software level, an iterative calibration approach is used. When determining the correction signal needed, the radar is swept while pointed at an empty scene and the return captured. This sweep correction signal is then calculated and applied in inverse to the unit. By placing the correction injection point prior to most of the system gain the ADC can be corrected beyond its' normal saturation level. This means the CCC generated by the DAC can correct many full scale ADC ranges. This is why an iterative calibration is needed. Only one full ADC

range correction should be applied per iteration, and so it may take many iterations to get the signal inside the ADC range for the final correction.

It is also important to ensure that the radar unit does not saturate before the correction. If the unit saturates before the correction is applied the correction does not provide any benefit. This applies a system level constraint on the unit that the self-interference must not push the pre calibration stages (LNA/Mixer) into saturation which can be a challenge for small radar units. For example, assuming a 0 dBm transmit output signal and -60 dB antenna-referred coupling, the maximum LNA gain ahead of the mixer would be 40dB if the mixer's input compression point is -20dBm. The hardware design was performed with these details accounted for.

4.2 - Revision A

Revision A of the radar (left side of Figure 4-1) was first built in early spring of 2017. It has a maximum theoretical frequency range of 23.5GHz-26.5GHz as constrained by the VCO inside the core chip with two receive channels and one transmit channel. The original concept for the two receive channels was that cross pole antenna measurements may have agricultural value later. The output was connectorized to be accessible via three edge launched SMP connectors. The system had an overall receive gain of 52dB that was adjustable by 0-40dB with a programmable gain amplifier (PGA) in the baseband stage to increase the systems dynamic range.

The frequency synthesis in revision A operates in an open loop manner. The tune voltage on the VCO is directly controlled via a digital to analog converter (DAC). The DAC was set to a voltage which corresponded to a desired output frequency. This was eventually determined to be the biggest issue with revision A, as sufficient open-loop frequency accuracy was difficult to achieve across a full sweep. The block diagram in Figure 4-2 is very similar to the

implementation for revision A except for the Phase Locked Loop (PLL) and loop filter feeding which were replaced with a DAC directly feeding the VCO.

The output frequency sweep accuracy needed to be improved. If the output frequency is slightly off from the desired, an offset phase return is collected. These slightly erroneous phase returns build and add noise into the processed returns. Part of this issue is due to the nonlinear tuning curve of the VCO, but also its' temperature dependence. This was corrected by sweeping the radar unit on a spectrum analyzer and evaluating the DAC state versus the output frequency. With this curve known, a reasonably linear frequency chirp could then be generated, but was sub-optimal relative to the performance achieved with later synthesized versions.

The realized hardware of version A was split into two PCBs. The main board seen in Figure 4-3(a) contained everything except for the voltage regulators which are contained on a separate board which can be seen in Figure 4-3(b). The system was controlled with a Teensy 3.6 microcontroller development board. The microcontroller controlled the frequency stepping via a 14-bit DAC over a serial peripheral interface (SPI) interface. It also controls two PGAs in the baseband chains to allow for a wider dynamic range. The analog to digital conversion was performed using a 16-bit ADC.

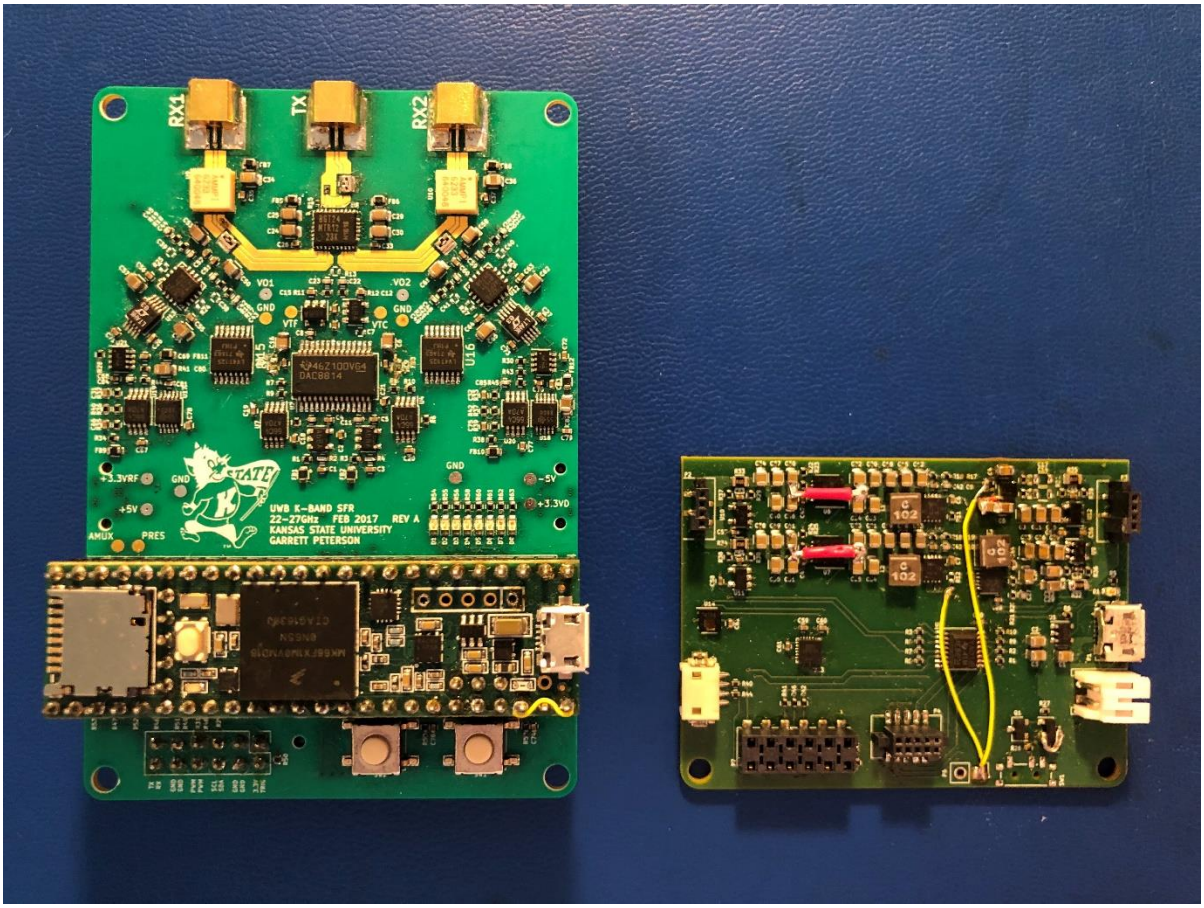

Figure 4-3 K-State Agricultural Radar Rev A RF Board(a), Power Board (b)

The main PCB is a 6-layer laminate with Rogers 4350B on outer layers and a normal FR4 on inner layers. A stackup of the board can be seen in Figure 4-4(a). The Rogers material was used as it was thought to be a good RF substrate for low loss and is well characterized. Some additional strategies to limit system self-interference were the use of CPWG transmission lines to limit line crosstalk. Additionally additively manufactured shields were created that could enclose the sensitive transmit and receive line sections in the hope of achieving isolation values approaching that of stripline. The shields were fabricated by research partners at the University of Arkansas. The antennas used with this initial system are additively manufactured Vivaldi

antennas provided by Michigan State University. The shields and antennas can be seen in Figure 4-5.

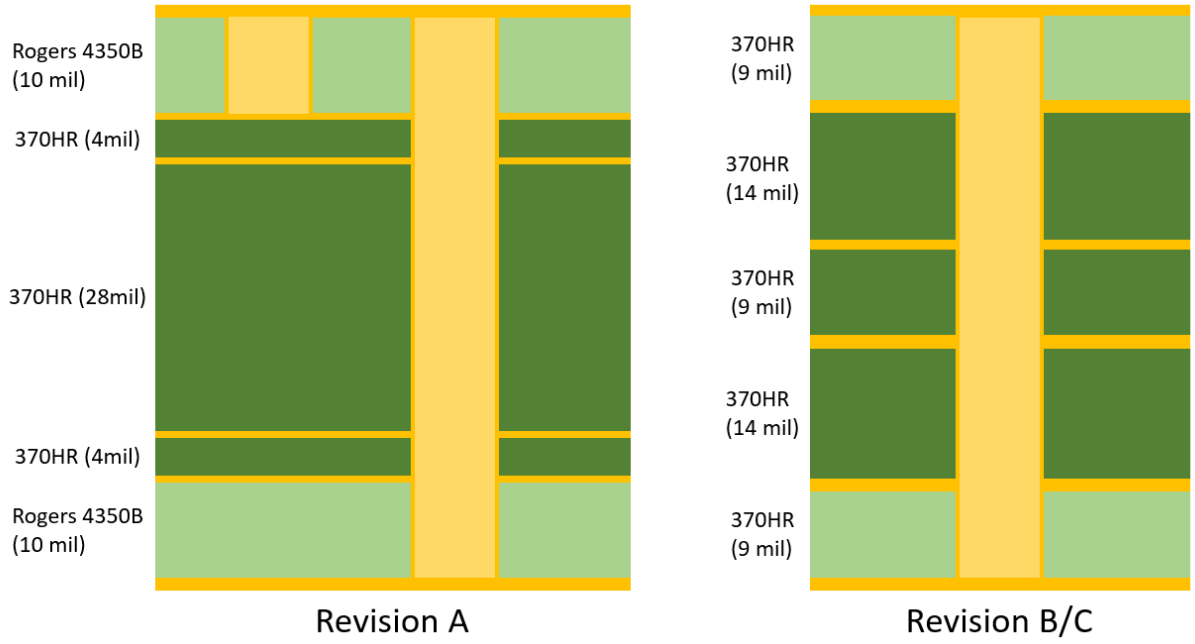

Figure 4-4 K-State Agricultural Radar PCB Stackups

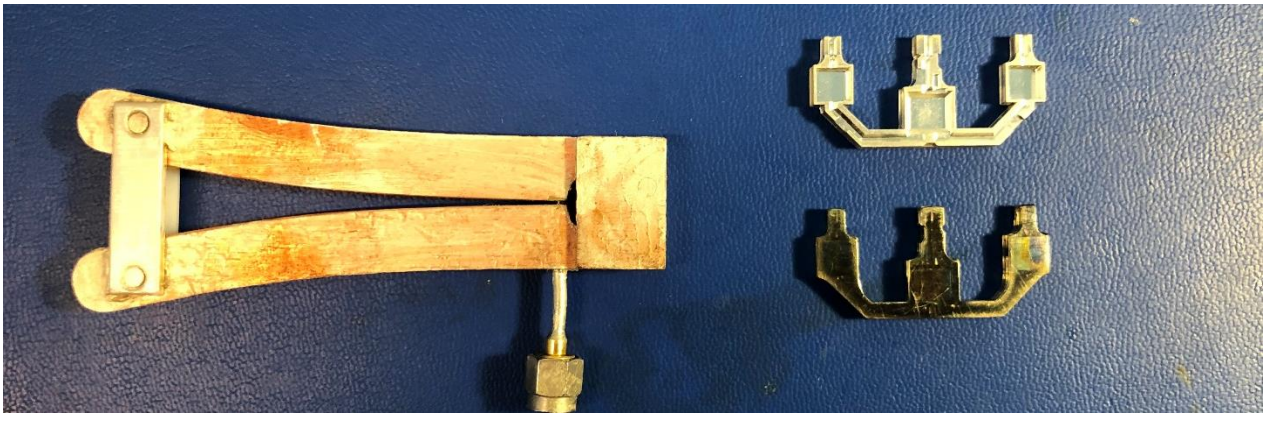

Figure 4-5 Additively Manufactured Antennas (from Michigan State University) and Shield Cover (from University of Arkansas)

4.3 - Revisions B/C

Revisions B and C of the radar are similar with a few modifications including a part change for the LNA and some layout corrections. These revisions also had a large departure from revision A with regards to the frequency synthesis and control. Using the same core chip it operated over the same frequency range with some small changes to the overall receiver gain and system noise figure. A block diagram of the analog board can be seen in Figure 4-2.

The frequency synthesis is the major change in regards to system operation. In the previous revision the output frequency was controlled using a DAC. In revisions B and C a PLL is added to increase the accuracy and repeatability of the sweep. To create the frequency steps needed for SFCW operation the divider inside the PLL was stepped in a manner to create the linearly stepped output waveform.

Digitally there is also significant change from revision A to B/C. The Teensy 3.6 microcontroller used on revision A was replaced with an Altera Max 10 field programmable gate array (FPGA). The state machine nature of the control code lended itself to an FPGA design flow well and allows for faster sweeping and better timing control in the radar. The FPGA also helps data transfer off the unit faster. The digital board for revisions B and C utilizes a USB 2.0 High speed interface that enables data transfer rates up to 480Mbps. This allows for faster data transfer from the radar unit to the computer where data processing is performed. The digital control board also houses the voltage converters and regulators. The RF board required +/-5V and a 3.3V supply. Revisions B and C utilized a buck/boost converter to create a stable 5.5V that was then linearly regulated to 5V and +3.3V. An inverting converter also created a -5V supply.

4.3 – Software Interface

The software interface to configure and control the radar unit is written in python. It communicates to the radar over the USB interface. It allows different frequency ranges, step dwell times, step sizes, and receiver gains to be configured. This information is transferred to the FPGA and then used to set various registers and program the PLL dividers and steps. The interface also allows for live plotting of the return data. Once the radar completes a sweep it transfers the data over USB to a computer running the python code. The computer can then plot the time domain waveform, calculate and plot the FFT waveform, and save the raw return data as csv files for further processing at a later date. This software enables real-time evaluation of the system. The software also allows for continuous sweeping by sending commands to sweep once data is returned. It also sends calibration commands to set the radar into a mode to perform the CCC calibration. The graphical user interface (GUI) can be seen in Figure 4-6 below.

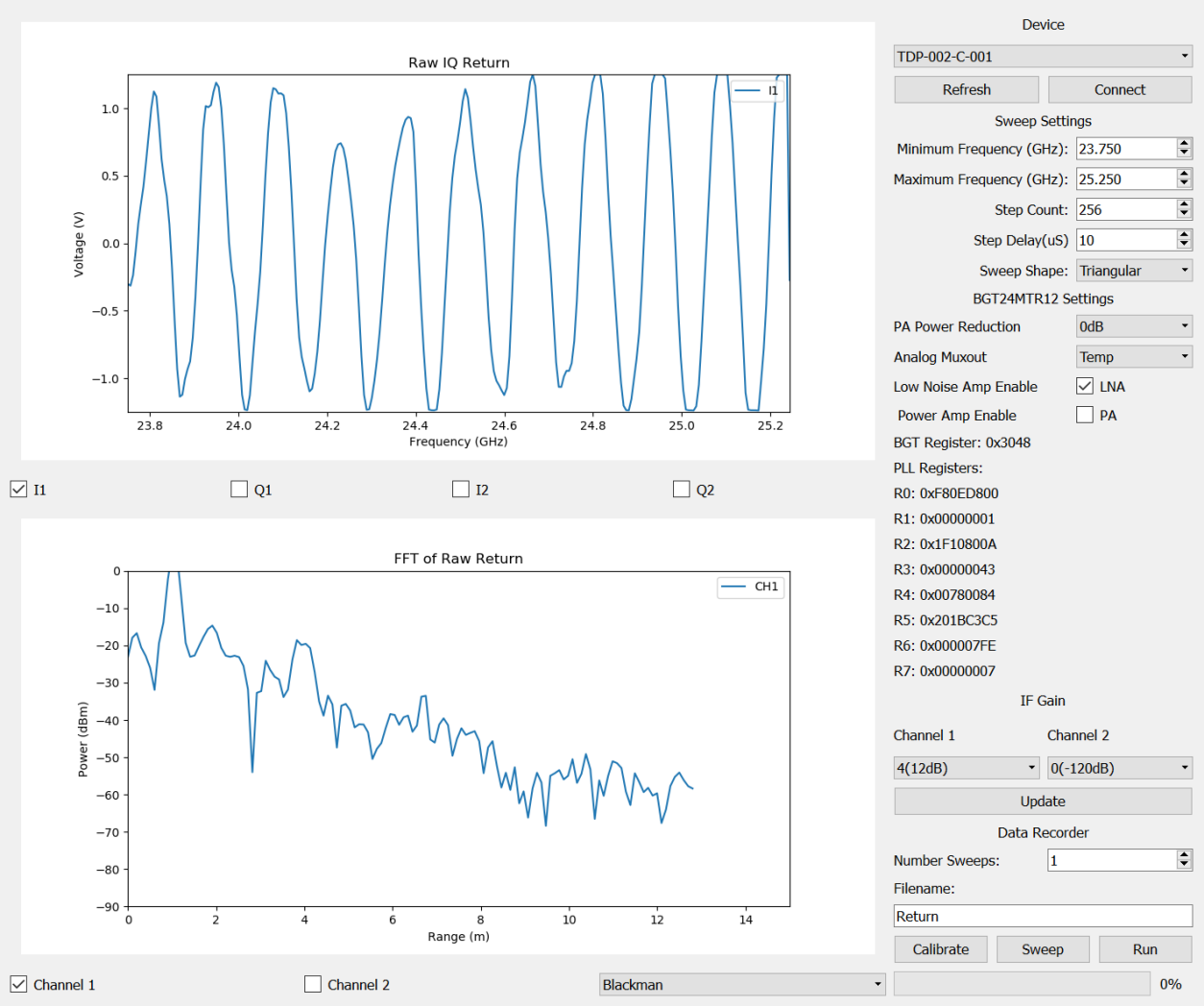

Figure 4-6 Software GUI Interface

Chapter 5 - Experimental Results

An example of an un-calibrated return from the radar while looking at a blank target-scene is shown in Figure 5-1 in the solid blue line. As can be seen, the IF/baseband output from this sweep produces around a half of a cycle of a low-frequency sinusoid, which can be correlated to a time-delay consistent with leakage through the mixer and a reflection off the LNA in this system. With an assumed dielectric constant of 4.2 for the PCB dielectric constant this distance can be determined to be approximately 4 cm. A slight DC offset can also be seen and is consistent with a zero-delay, from on-chip coupling in the primary RF chip from internal structures such as matching inductors for amplifiers in the transmit and receive path. A calibrated return with CCC applied can be seen in in the dashed blue line in Figure 5-1. This shows the CCC corrections can account for significant leakages.

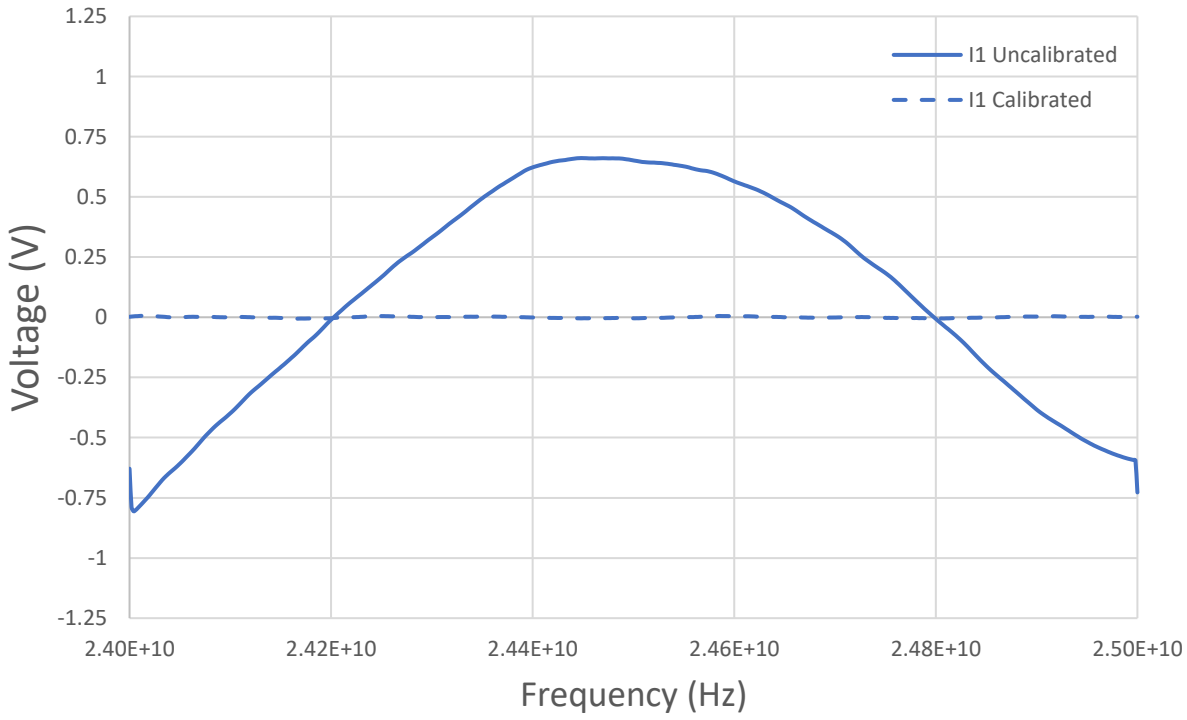

Figure 5-1 Example Radar Return

The waveform in Figure 5-1 was taken from the ADC input point in the receive chain, with a minimal IF gain after mixing to keep the voltages within the ADC-range. Clearly the coupling leading to this waveform is substantial. Measurements of the transmit signal levels that were present in the receive line were performed on a revision C board to evaluate the isolation between transmit and receive sections. It was found that this isolation was around 20dB. The measurement was taken by probing the transmit line with an active microwave probe and a spectrum analyzer to see the output power and then probing one of the receiver lines post external LNA to see the relative level of the signal. The probe was moved around to eliminate the possibility of standing waves affecting recorded values. The test setup to measure the isolation can be seen in Figure 5-2. These measurements occurred with the transmit and receive antenna ports terminated to minimize any radiation coupling from the transmit port to the receive port.

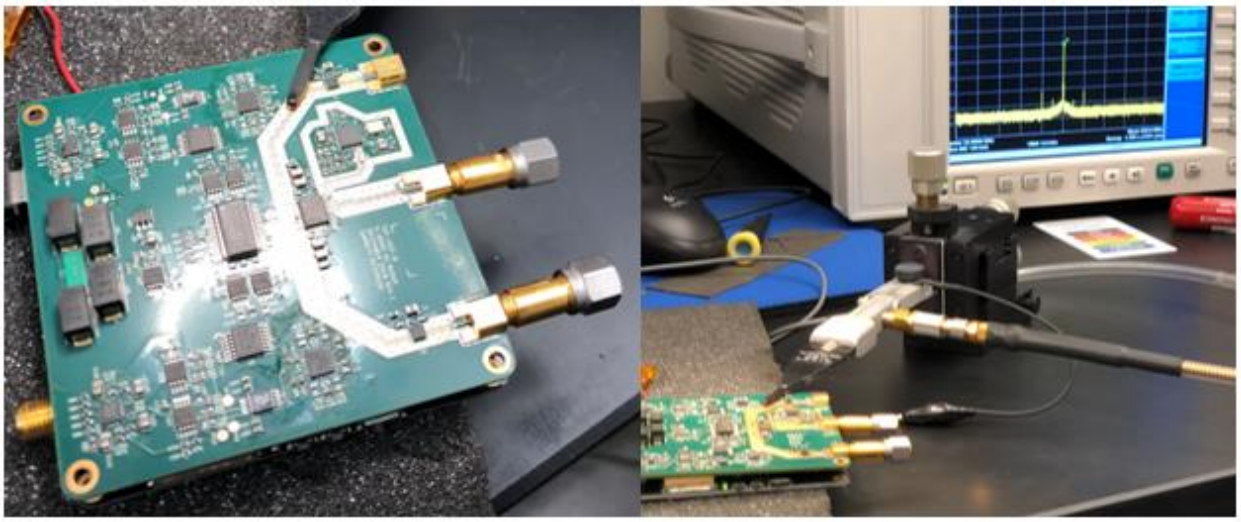

Figure 5-2 Transmit/Receive Leakage Measurement Setup

Measurements to determine the minimum detectable signal were also performed. The transmit signal was fed through a variable attenuator and sent through a length of coaxial cable. This cable simulated delay and attenuation that would normally occur as the signal propagated

and returned through the air. This is conventionally called a loopback test. The attenuator was increased until the signal was not discernable from the noise. It was found that the minimum discernible signal was -115dBm input antenna referred power. This is close to the theoretical noise floor of -120dBm given a 100KHz receive bandwidth and a 4dB noise figure.

5.1 - Real World System Performance

A simple over the air test was performed to verify radar operation and the CCC technique in implementation. The radar was sited in an interior environment and pointed to view some absorbing foam placed on the floor. The absorbing foam was used to mitigate some real world non idealities for initial tests. Calibrations of the scene including the absorbing foam were then performed. A plot of the real iterative calibration process during this test can be seen in Figure 5-3. The initial calibration iteration is the thinnest/lightest line and the final is the thickest/darkest line. We can see the calibration correcting beyond the saturation point and into the ADC range. Gradually this brings the returns close to zero for the thickest lines. There is a slight overcorrection on each iteration due to a slight gain non-ideality in the physical system. After 10 sweeps and calibrations applied the output was negligibly small.

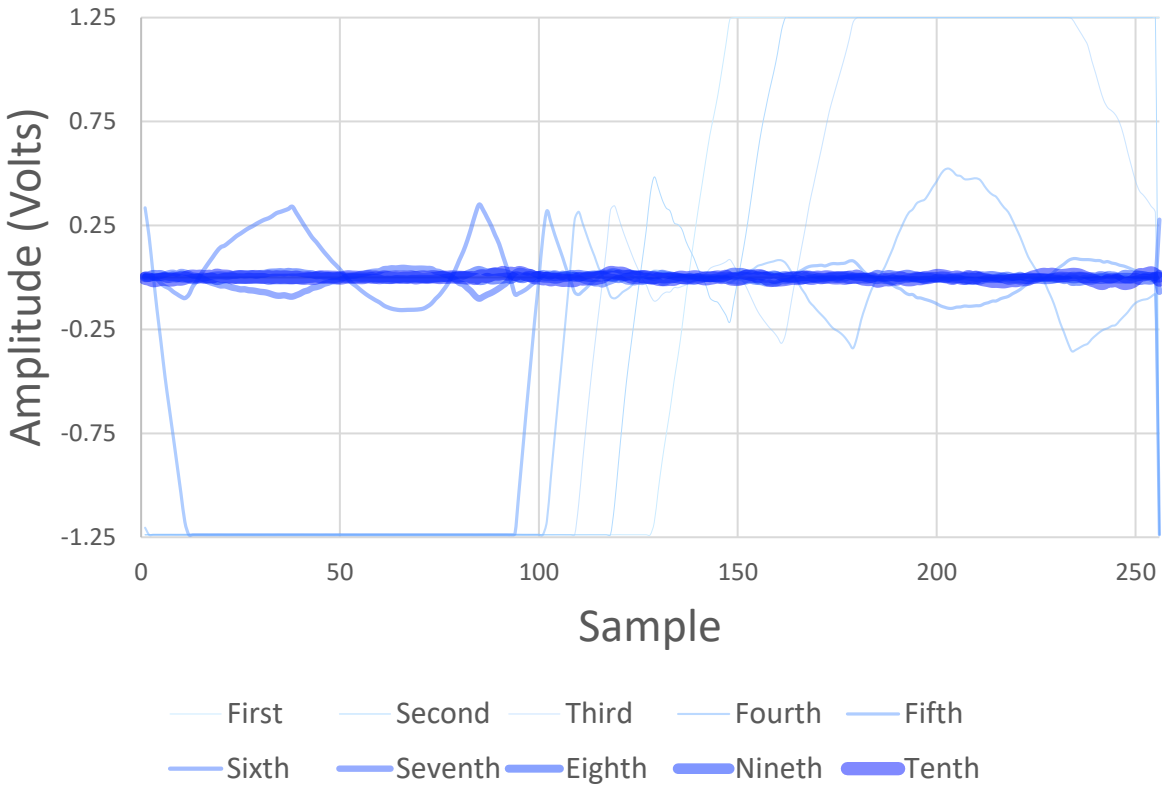

Figure 5-3 Iterative Calibration Process

Once the calibration was verified, small spherical targets were placed in the scene. The targets were Styrofoam balls wrapped in aluminum foil. The resulting metal spheres had calculated radar cross sections (RCS) of 0.03, 0.015 and 0.07 meters squared respectively. Scenes where then captured with the targets. The test setup can be seen in Figure 5-4.

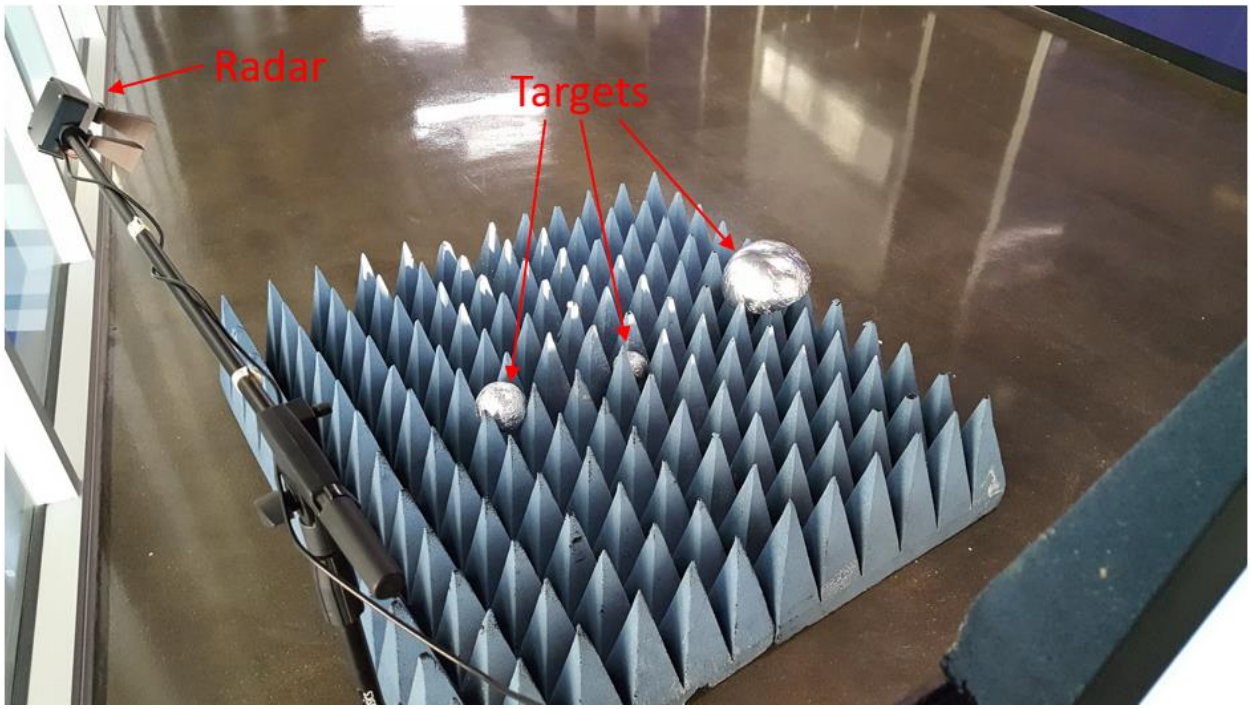

Figure 5-4 Multi-Target Test Setup

Plots of the processed returns are shown in Figure 5-5.The top plot shows the processed return post-calibration with no targets present. Ideally this plot should be a completely empty return, and the success of the calibration is indicated by the lack of any significant low-frequency sinusoids showing up in the FFT plot. The second plot shows is a processed return with the closest target inserted. The third plot shows a return with two targets. The bottom plot shows the results with all three targets. Looking at these figures we can see the addition of each target and the radar's ability to resolve individual targets even with relatively close distances. A Hamming window was applied to these returns.

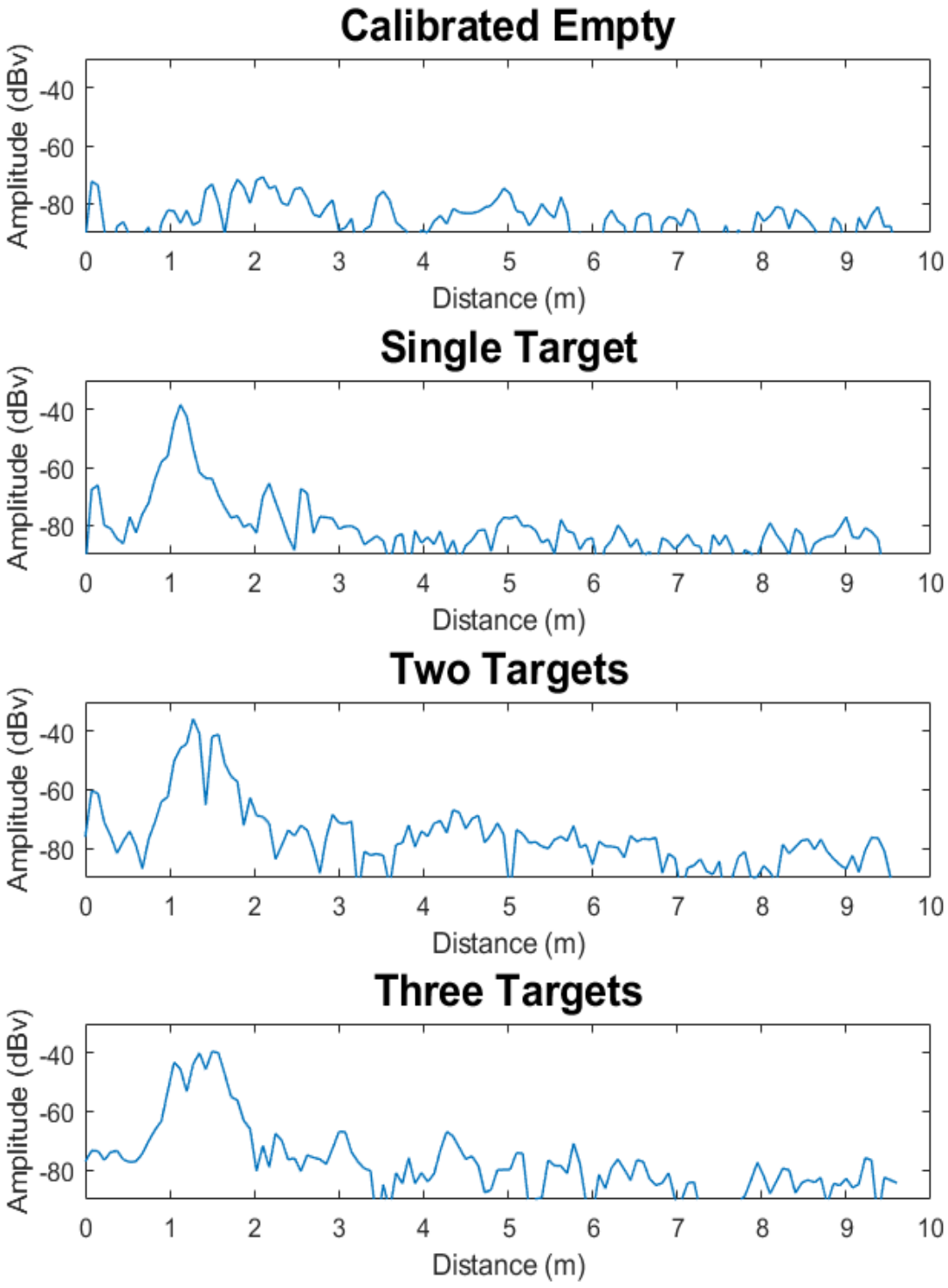

Figure 5-5 Processed Multi-Target Returns

5.2 - Agricultural Field Experiments

Various field experiments were performed at Kansas State University's Ashland Bottoms research farm to assess the abilities of the radar in actual agricultural applications. Trials conducted looked at different radar system settings as well as different crops. Some of the different crops included soybeans, grain sorghum, and corn. The experimental setup had the radar extended on a boom looking up towards an open sky for calibration and down towards the crops in the tests. A photo of early soybean experiments in action can be found in Figure 5-6. In this photo the radar can be seen taking measurements at the end of the boom in a white enclosure. The radar was truthed between trials to ensure that the CCC still showed a reasonably empty return when pointed towards the sky. If the calibration had drifted beyond a reasonable amount the unit was recalibrated.

Figure 5-6 Early Soybean Experiment Setup

5.2.1 - Early Soybean Field Trials

Some of the early field trials were just testing basic field performance. The initial tests were in September of 2018 and looked at soybeans. These were some of the first measurements using revision B. A small patch array was used for each antenna as seen in Figure 5-7. Some absorbing material was added to the backside of the antennas to mitigate the back radiation and improve the calibration with an empty sky. The test results from these trials shown Figure 5-8.

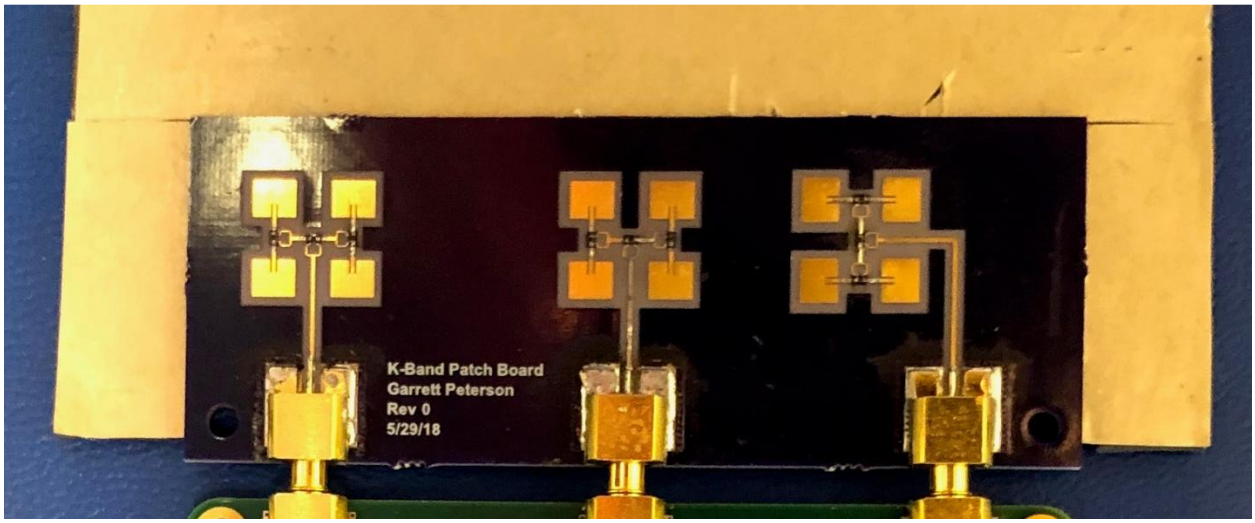

Figure 5-7 Ag Radar with Patch Antenna Arrays

This early test involved some ground-only target verification to see basic operation before moving over the crop. The system was first pointed up towards the sky to perform the CCC. Once the unit was calibrated and verified the antennas were pointed towards some empty ground. In the annotated spectrogram found in Figure 5-8 the unit starts over empty ground before being lowered toward the ground. It was then raised up, moved over the soybeans, lowered close to the canopy of the crop and moved away. These spectrograms show the data as intensity at distances over time. The y-axis represents a distance from the radar while the x-axis is a pseudo time axis. Here the x-axis represents the sample number where each sample is a complete radar sweep. The spectrogram is built by taking a Fourier transform of each sweep and

showing the spectrum (which equates to range) as a vertical strip, with a color representing intensity. This early test showed the radar functionality and verified successful operation of the CCC on the unit. It also showed some need for performance improvement needed to see the ground below the crop canopy.

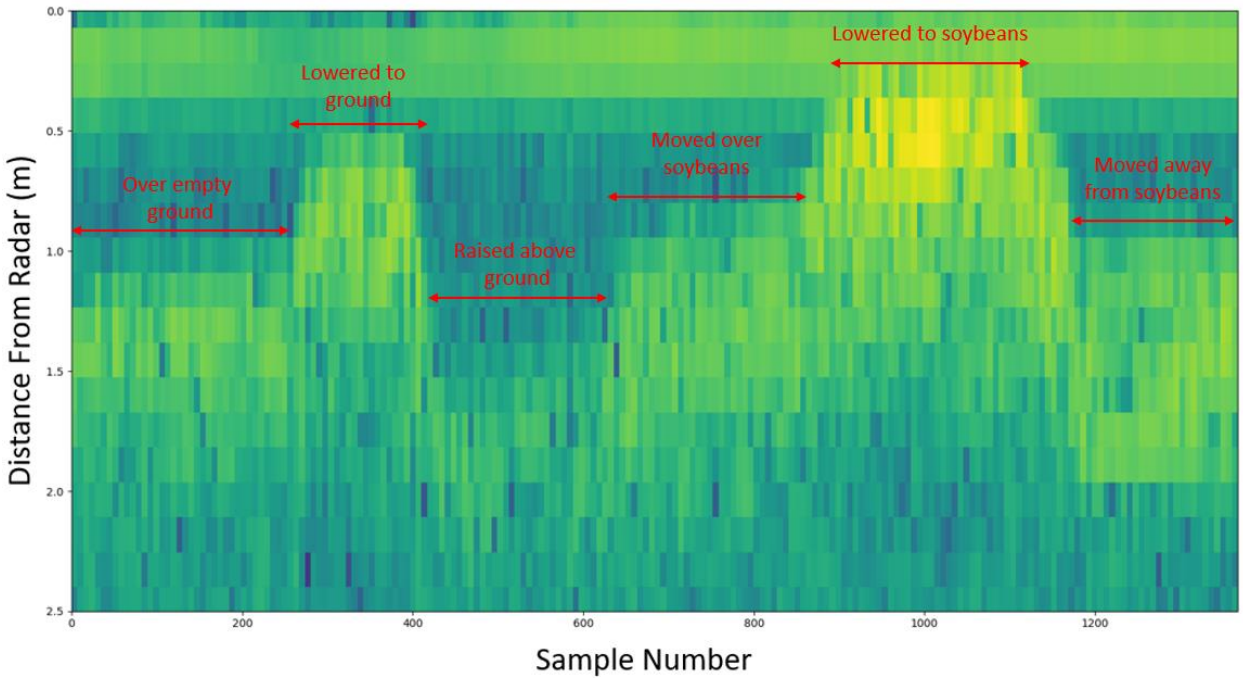

Figure 5-8 Early Soybean Spectrogram

5.2.2 Additional Crop Trials

After these successful initial trials, improvements were made to the radar to address some issues that were discovered. Improvements included increased gain, refined frequency synthesis, improved antennas, and low-pass filter corner frequency filter adjustments. The crop trials shown in this subsection were taken using a Rev C version of the radar using the 3D printed horn antennas previously shown in Figure 3-2. Data shown here was taken during September of 2019.

Data was taken over soybeans again to compare against previous trials as well as grain sorghum and sweet corn. Data is displayed in a spectrogram, as before, but with improved color scaling and using timestamps for the X-axis. Some upscaling interpolation was also used to smooth the data bins and improve the color transitions. Figure 5-9 and Figure 5-10 show the difference the upscaling can do to make data easier to interpret. The soybean data in those figures also shows some crop injury that had occurred on plants as part of an agricultural experiment being performed at the test-site for herbicide drift damage. The injury in the experiment can be seen as a variation in crop height with the most severely injured crop measurements around 9:14:50.

Some deterioration of the CCC corrections can be seen in Figure 5-10. This is a result of some calibration drift since the calibration was performed and shows as a close-range (0.5m) spurious target resulting in some cable flex to the antenna. This drift comes from temperature but also some cable flex in the unit.

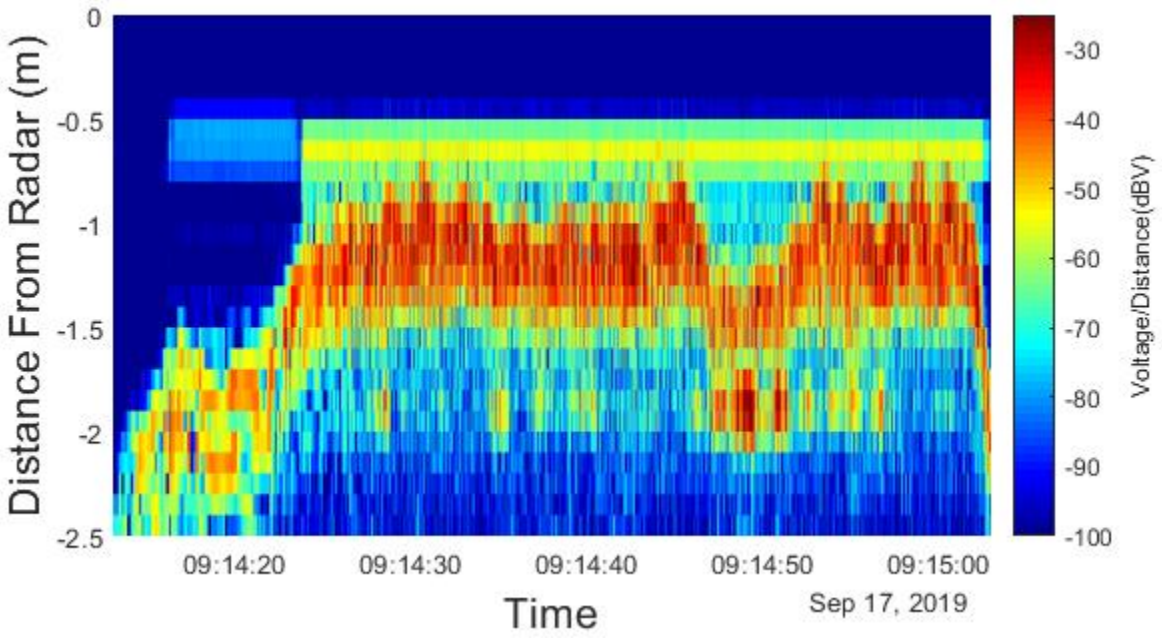

Figure 5-9 Rev. C Injured Soybean (Raw)

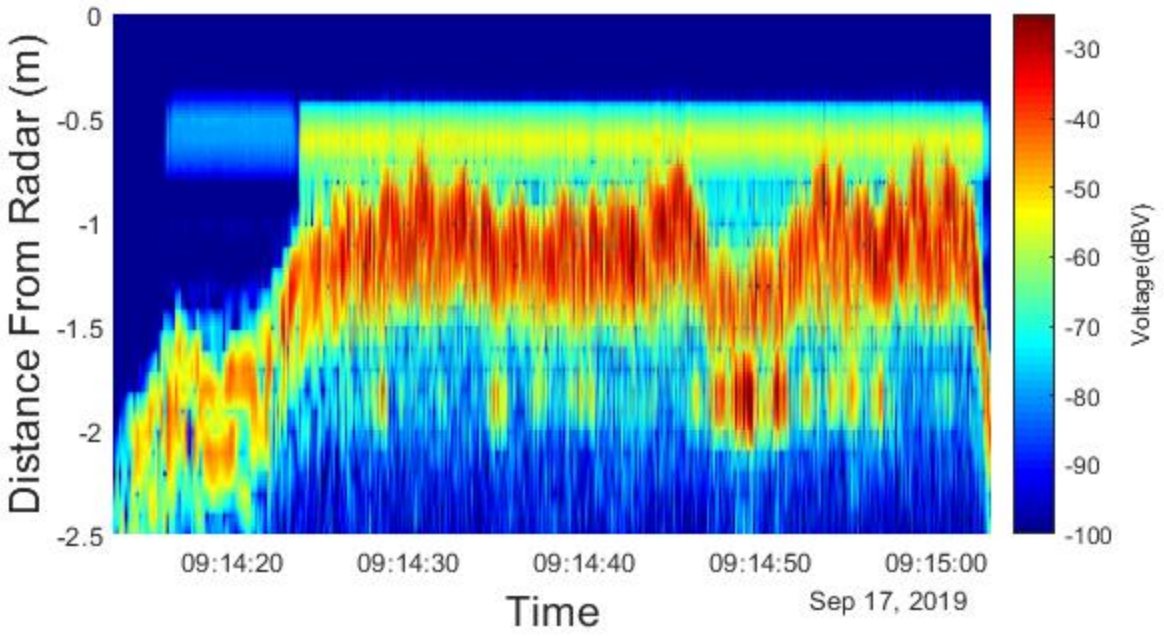

Figure 5-10 Rev. C Injured Soybean (Upscaled)

These experiments were conducted by attaching the radar to a boom sticking out from a vehicle above the crops and driving along the edge of the field. It should be noted that these trials were conducted by moving the radar perpendicularly across the rows and not in parallel. Ground returns can also be seen around the 1.75 meter distance from the radar. It is noticeably more visible during the injured crop portion where the canopy was not as developed and the radar had a better view of the ground rows between plants. An example of the vehicle mounted experiment setup for sorghum measurements can be found in Figure 5-11. The radar boom is mounted of the passenger side just above the crop.

Figure 5-11 Sorghum Vehicle Mounted Experimental Setup

These trials highlight some of the radars strengths and what the best modes of operation should be. A spectrogram of the sorghum trial can be found in Figure 5-12. In the sorghum trials the top of the crop was a tassel full of grain during the measurements and was visible sticking out from the canopy in the return. Most of the canopy of the crop was around 1 meter away from the radar but the grain heads can be seen above the canopy with peaks around 0.5 meters away from the radar as it traversed the rows. Ground returns can also be seen between the rows at a 2 meter distance from the target.

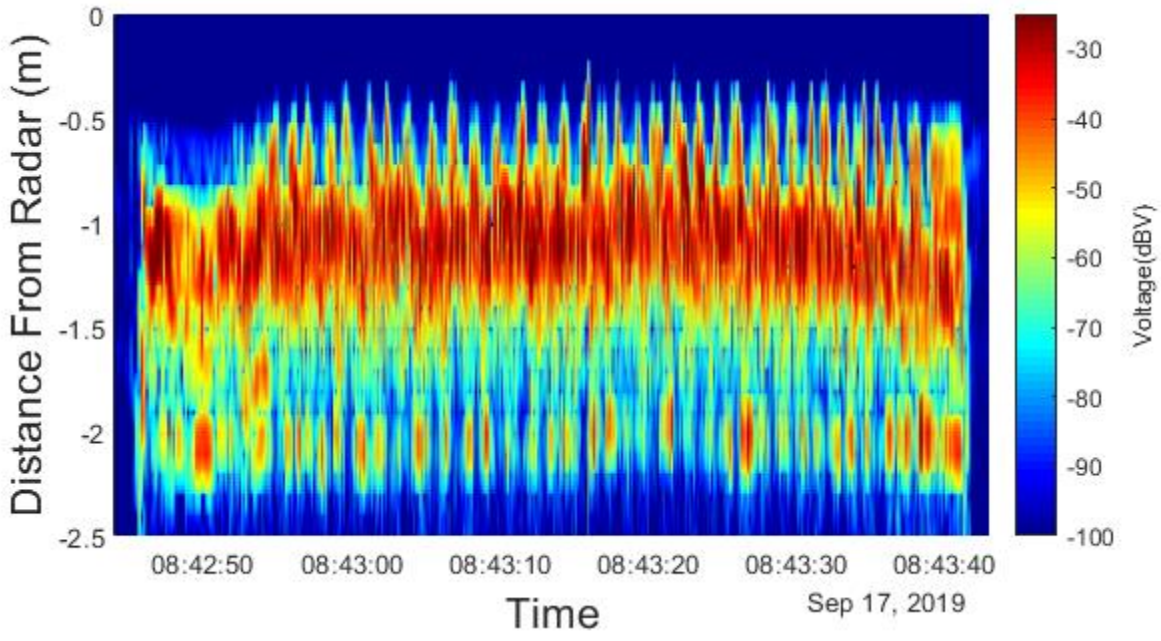

Figure 5-12 Rev. C Sorghum Experiment

These spectrograms of sorghum show a good potential for easy crop height measurements as well as give some idea of the crop head size. The sorghum head which sticks out of the canopy is the harvested portion of the crop and thus can be used to make yield estimates. A side view of some of the sorghum plants used in the experiment can be found in Figure 5-13.

Figure 5-13 Sorghum Crop Side View

The last crop looked at during that experiment session was sweet corn that was at late stages of life. It was sparsely populated and thus highlighted more of the ground versus crop

height returns. The spectrogram for those results can be seen in Figure 5-14.Again a strong return from some cable flex appears around 0.6 meters.

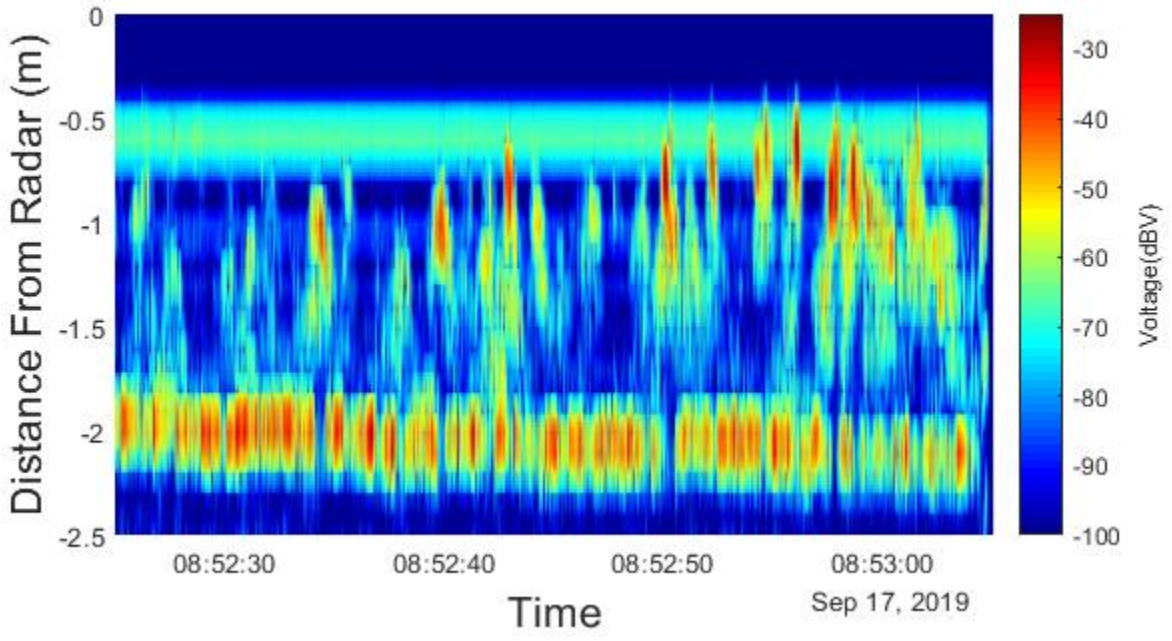

Figure 5-14 Rev. C Sweet Corn measurements

These later field experiments show great promise for the experimental radar's ability to measure absolute crop height and crop biomass, but also illustrate some of the radar strengths and weaknesses. The reflectivity of the crops at 24GHz provides strong returns from the crop, but can lead to weak ground returns given a full canopy. The experiments also showed how different crop types can result in varied returns. The radar in its current form will therefore be more useful for some crops that others. Grain Sorghum provided some of the most interesting returns in regards to yield estimate data.

Chapter 6 - Conclusions and Future Work

Short-range radars must address coupling between antennas and traces/circuit-elements in a hardware implementation to be able to resolve close-in targets. This has historically been a unique case as most radars look at long range targets such as aircraft or weather phenomena with some exceptions. Most of the coupling issues result in short range false targets can be either filtered or range gated out to solve the issue for long/medium range systems, but the issue remained for short-range systems.

In this work it was shown that CCC mitigation can greatly reduce the effects of self-interference in short-range systems. It has been evaluated with a hardware implementation through the development of the K-State Agricultural radar. It has shown interesting promise for indoor monitoring by being able to mitigate unwanted multipath returns as well as provide very short range radar measurements.

It was also seen that a very static system was required to make calibrations valid. Any physical changes to the system can make changes to the crosstalk/leakage in the system and the calibration can be corrupted. This issue is still open for temperature compensation, but can be addressed in the physical implementation. Work has started to physically implement an integrated antenna system into the radar units to minimize or eliminate any connector flex or cable flex issues. A PCB mounted waveguide solution has been developed and shows promise as a connectorless solution. In future radar revisions this will be integrated into the board. A picture of a prototype solution can be seen in Figure 6-1.

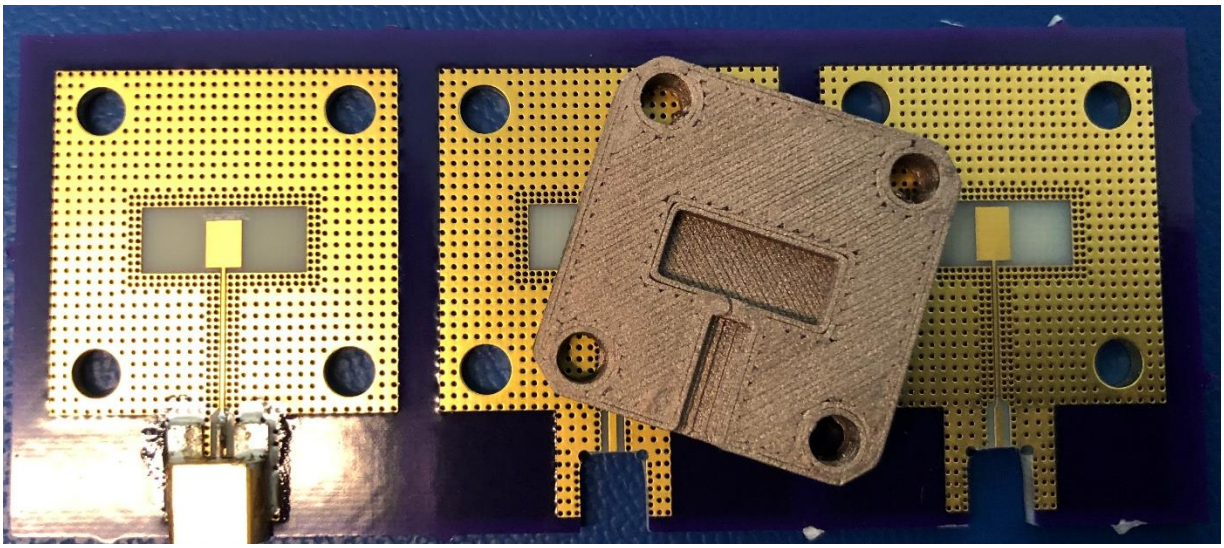

Figure 6-1 Connectorized PCB Waveguide Adapter

In addition it was found that the frequency band used at 24GHz could not fully penetrate thick canopies. The author believes that this is due to the reflectivity of the crops at this frequency. More studies need to be performed at different frequencies to evaluate practical canopy penetration of different spectrums. This could help future agricultural radars obtain more accurate measurements and more crop-health information.

The K-State agricultural radar has shown promise as a tool to gather data on crops. Several field trials were conducted on various crops to evaluate real world returns and see what kinds of data sets are possible. The field experiments showed crop heights were easily obtained given a mildly dense canopy. One suggested method is to run in parallel with crop rows to gather returns from both crop and ground to make absolute crop height measurements. The experiments also showed some promise of yield estimates by providing the head height of grain sorghum. This still requires further evaluation and correlation between measured yields and radar measurements. It will likely also vary by sorghum variety.

More field trials also need to be performed to fully understand and correlate the radar returns to the specific crop measurements needed by growers. This kind of measurement systems

could also be employed of a larger scale in a remote monitoring solution such as a drone to easily show stunted growth in a field. The hope is that with more data growers can develop better growing practices to increase crop yields.

References

[1] G. L. Charvat, *Small and Short-Range Radar Systems*, Boca Raton: CRC Press, 2014.

[2] M.-K. Olkkonen, P. Eskelinen, E. Huuskonen-Snicker, T. Pellinen and P. O. Martinez, "A New Microwave Asphalt Radar," in *2014 International Radar Conference*, Lille, 2014.

[3] Vayyar Imaging, "DIY: Walabot," [Online]. Available: https://walabot.com/diy. [Accessed 15 July 2020].

[4] R. Lachner, "Development Status of Next Generation Automotive Radar in EU," in *ITS Forum*, Tokyo, 2009.

[5] United Nations, Department of Economic and Social Affairs, Population Division, "World Population Prospects:Highlights," United Nations, New York, 2019.

[6] PrecisionAg, "PrecisionAg," PrecisionAg.com, 20 October 2015. [Online]. Available: https://www.precisionag.com/market-watch/precision-agriculture-terms-and-definitions/. [Accessed 6 June 2020].

[7] Lucintel, "Agriculture Robot Market Report: Trends, Forecast and Competitive Analysis," 2019.

[8] T. L. Toan, A. Beaudoin, J. Riom and D. Guyon, "Relating Forest Biomass to SAR Data," *IEEE Transactions on Geoscience and Remote Sensing*, vol. 30, no. 2, pp. 403-411, 1992.

[9] J. Hasch, E. Topak, R. Schnabel, T. Zwick, R. Weigel and C. Waldschmidt, "Millimeter-Wave Technology for Automotive Radar," *IEEE Transactions on Microwave Theory and Techniques*, vol. 60, no. 3, pp. 845-860, 2012.

[10] D. Korpi, L. Anttila, V. Syrjala and M. Valkama, "Widely Linear Digital Self-Interference Cancellation in Direct-Conversion Full-Duplex Transceiver," *Selected Areas in Communications*, vol. 32, no. 9, pp. 1674-1687, 2014.

[11] S. Hong, J. Brand, J. I. Choi, M. Jain, J. Mehlman, S. Katti and P. Levis, "Applications of Self-Interference," *IEEE Communications Magazine*, vol. 52, no. 2, pp. 114-121, 2014.

[12] J. I. Choi, M. Jain, K. Srinivasan, P. Levis and S. Katti, "Achieving Single Channel, Full Duplex WirelessCommunication," in *16th Annual International Conference on Mobile Computing and Networking*, Chicago, 2010.

[13] M. A. Richards, J. A. Scheer and W. A. Holm, *Principles of Modern Radar: Basic Principles*, Raleigh: Scitech Publishing, 2010.

[14] R. Garg and I. J. Bahl, "Characteristics of Coupled Microstriplines," *Transactions on Microwave Theory and Techniques*, vol. 27, no. 7, pp. 700-705, 1979.

[15] T. Rider, W. B. Kuhn and A. Wolf, "Crosstalk and EMI in Mixed-Signal / Microwave Multi-Layer PC Boards," in *International Symposium on Electromagnetic Compatibility & Signal/Power Integrity (EMCSI)*, Washington DC, 2017.

[16] A. Abramowicz, "New Model of Coupled Transmission Lines," *Transactions on Microwave Theory and Techniques*, vol. 43, no. 6, pp. 1389-1392, 1995.

[17] T. W. Rider, "Crosstalk and EMI on microwave circuit boards," M.S. thesis, Kansas State Univ., Manhattan, 2017.

[18] I. D. Sobering, "Mitigating oscillator pulling due to magnetic coupling in monolithic mixed-signal radio-frequency integrated circuits," M.S. thesis, Kansas State Univ. Manhattan, 2014.

[19] T. H. Lee, *Planar Microwave Engineering*, Cambridge: Cambridge University Press, 2004.

[20] Y. Naito and K. Suetake, "Application of Ferrite to Electromagnetic Wave Absorber and Its Characteristics," *Transactions on Microwave Theory and Techniques*, vol. 19, no. 1, pp. 65-72, 1971.

[21] G. Peterson and W. Kuhn, "Coherent calibration cancellation for stepped frequency radar systems," in *2018 IEEE Radar Conference*, Oklahoma City, OK, USA, 2018.

[22] D. M. Pozar, *Microwave Engineering*, Hoboken: John Wiley & Sons, Inc, 2012.